UNITED NATIONS UNIVERSITY
GEOTHERMAL TRAINING PROGRAMME
Orkustofnun, Grensásvegur 9,
IS-108 Reykjavík, Iceland

Reports 2009
Number 16

JOINT 1-D INVERSION OF TEM AND MT DATA FROM OLKARIA DOMES GEOTHERMAL AREA, KENYA

Charles Muturia Lichoro
Kenya Electricity Generating Company – KenGen
Olkaria Geothermal Project
P.O. Box 785, Naivasha
KENYA
cmuturia@gmail.com

ABSTRACT

Joint one-dimensional (1-D) inversion of magnetotelluric (MT) and central loop transient electromagnetic (TEM) data was done by fitting both data sets using the same 1-D resistivity model. It is well known that in the presence of small-scale surface or near-surface resistivity inhomogeneities the MT apparent resistivity can be shifted by a multiplicative factor which is independent of frequency. In this regard, for this project, TEM was used to correct for the static shift factor to restore the MT curve to where it should have been without the effects of shifting.

In the Olkaria Domes, the 1-D joint inversion results reveal three main resistivity zones, a shallow high-resistivity zone (> 100 Ωm) to about 300 metres below the surface, an intermediate-low resistivity zone (10 Ωm) to depths of about 1 km and a deeper high-resistivity zone (> 50 Ωm), up to 3-4 km depth. Below the high resistivity, a zone of relatively low resistivity at depth is evident, possibly indicating high temperature which may be associated with crustal fluids, a heat source for this field.

A good correlation is found between the resistivity structure, hydrothermal alteration and reservoir temperatures. The low resistivity is dominated by conductive minerals in the smectite-zeolite zone at temperatures of 100-200°C. In the temperature range of 200-240°C, zeolites disappear and smectite is gradually replaced by resistive chlorite. At temperatures exceeding 250°C, chlorite and epidote are the dominant minerals and the resistivity is probably dominated by the pore fluid conduction in the high-resistivity core, provided that hydrothermal alteration is in equilibrium with the present temperature of the reservoir.

1. INTRODUCTION

1.1 Scope of work

This report presents the geophysical work performed in Olkaria-Domes in Kenya at different times in the time interval from 2000 to 2009. It covers Magnetotelluric (MT), Audiomagnetotelluric (AMT) and Transient Electromagnetic (TEM) data acquisition, processing and interpretation using a one-dimensional (1-D) joint inversion of those data sets, where a damped (Occam) linear least-squares inversion program by Árnason (2006) is applied. The results are presented both by iso–resistivity

maps at different elevations and resistivity cross-sections along profiles. The goal of this study is to establish the resistivity structure of the Olkaria Domes field and correlate it with the alteration mineralogy and the reservoir characteristics from wells that have been drilled and suggest possible locations for future drill holes. The inversion code inverts for the static shift in the MT data using the TEM data measured at the same or a nearby location. The TEM data is not affected by such a shift since it does not measure the electrical field.

An attempt is also made to relate the modelled geophysical parameters to the geological and tectonic structures and the geothermal reservoir characteristics from wells in the area.

1.2 Geological and tectonic setting

The Olkaria Domes geothermal field is situated south of Lake Naivasha on the floor of the southern segment of the Kenya rift. The rift is part of a continental divergent zone where spreading occurs resulting in the thinning of the crust and, hence, the eruption of lavas and associated volcanic activities (Lagat, 2004). Olkaria Domes geothermal field is located on the southeast part of the Greater Olkaria geothermal area. The area is approximately bound by Ol'Njorowa gorge to the west and a ring of domes to the east and south of the field (Figure 1).

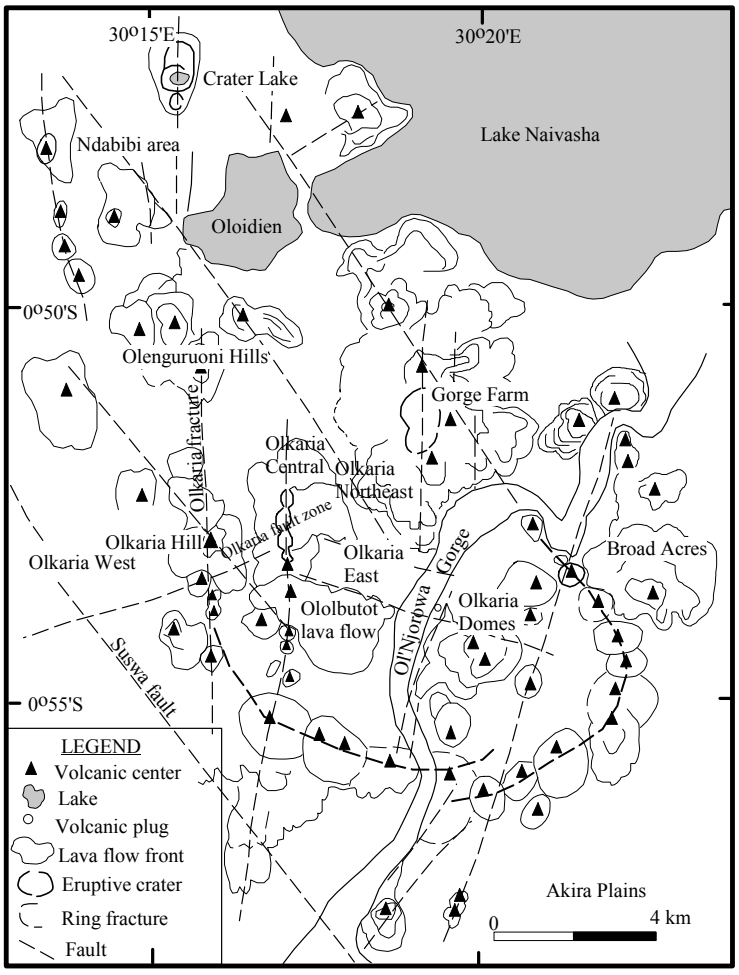

FIGURE 1: Volcano-tectonic map of the Greater Olkaria volcanic complex (modified from Clarke et al., 1990)

The Greater Olkaria volcanic complex is characterized by numerous volcanic centres of Quaternary age and is the only area within the Kenya rift with occurrences of comendite (a type of white rhyolite comprising the minerals amphibole and pyroxene) on the surface (Lagat, 2004). Other volcanoes in Kenya are associated with calderas of varying sizes. Olkaria volcanic complex does not have a clear caldera formation, which might suggest it is younger in age compared to other volcanic areas in Kenya. However, as seen in Figure 1, the volcanic domes in the east, south and southwest appear to be located on a ring shaped structure. This observation has been used to suggest the presence of a buried caldera (Naylor, 1972, Virkir, 1980, Clarke et al., 1990, Mungania, 1992). In support of the caldera theory micro-seismic studies have indicated possible attenuating bodies under the ring of Domes (Simiyu et al., 1998). Ignimbrite flows that could have been associated with the caldera collapse have not been positively identified in Olkaria (Lagat, 2004). Petrochemistry of lavas within the Olkaria area shows that they evolved from discrete magma chambers. Another explanation to the caldera hypothesis

would be that the ring structure was produced by magmatic stresses in the Olkaria "magma chamber" with the line of weakness being loci for volcanism (Omenda, 2000).

Magmatic activity associated with Olkaria volcanic complex commenced during the late Pleistocene and continues to Recent as indicated by Ololbutot comendite, which has been dated at 180±50 years BP using C^{14} from carbonized wood from a pumice flow associated with the lava (Clarke et al., 1990).

1.3 Structures controlling geothermal system in Domes area

The structures in the Olkaria domes geothermal field include among others the ring structure, the Ol'Njorowa gorge, and NW-SE and WNW-ESE trending faults (Figure 2). The faults are more prominent east and northeast of the Domes geothermal field and very few are visible within the Domes area itself, possibly due to the thick pyroclastic cover from the adjacent Longonot volcano which conceals fractures and hydrothermal manifestations. The NW-SE and WNW-ESE faults are thought to be the oldest and are associated with the development of the rift (Lagat, 2004). The most prominent of these faults is the Gorge Farm fault, which bounds the Olkaria-NE geothermal field in the northeast part and extends to the Olkaria Domes field. Hydroclastic craters located on the northern edge of the Olkaria Domes area mark magmatic explosions which occurred in submerged country (Mungania, 1999). These craters form a row along which the inferred caldera rim trace passes (Figure 1). Dyke swarms exposed in the Ol'Njorowa gorge trend in a north-northeasterly direction, further attesting to the recent reactivation of faults with that trend. Subsurface faults have been encountered in most Olkaria wells as reported in geological well reports (Lagat, 2004). Drilling problems have been reported whenever these faults were dissected due to cave-ins and loss of drilling fluids and cement. Materials collected when the circulation of the drilling fluid was normalized were mainly fault breccias.

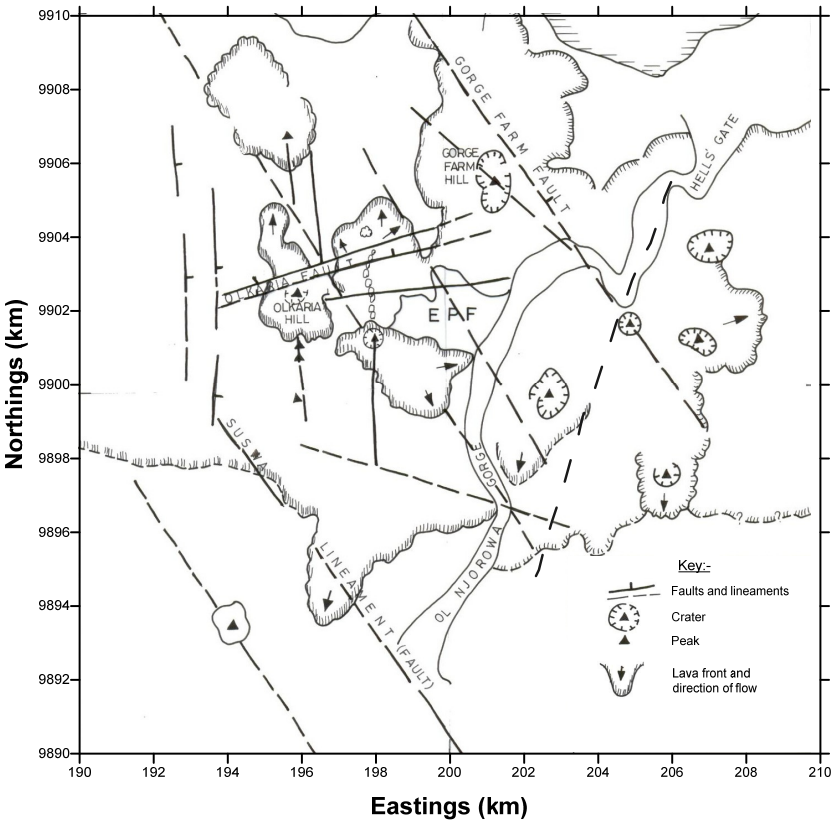

FIGURE 2: Structural map of the Greater Olkaria geothermal area (modified from Muchemi, 1992)

2. APPLICATION OF RESISTIVITY METHODS IN GEOTHERMAL EXPLORATION

Electrical resistivity methods have proven to be useful tools in geothermal exploration for a long time now. This is because they relate directly to the properties that characterize geothermal systems such as permeability, porosity, salinity, temperature and degree of hydrothermal alteration of the rocks (Hersir and Björnsson, 1991). Geoelectrical measurements provide information on the distribution of

the subsurface electrical resistivity. In high-temperature geothermal systems, electrical resistivity variations are often predominantly caused by hydrothermal alteration zones (Árnason et al., 2000). The hot fluids of a geothermal system lead to the formation of a sequence of hydrothermal alteration minerals dependent on temperature.

Resistivity methods are used to determine variations in electrical conductivity of the sub-surface, both laterally and with depth. Electromagnetic (EM) methods are more sensitive to conductive (low-resistivity) structures compared to direct current (DC) techniques. Among the methods used are MagneoTtellurics (MT) which uses natural-source signal and the Time domain ElectroMagnetic method (TEM) which uses a controlled-source signal.

Some resistivity methods have been applied in geothermal resource assessment for several decades. In DC resistivity sounding, an electrical current is injected into the ground and the potential voltage generated by the current distribution in the earth is measured at the surface. The DC method is more sensitive to resistive structures, hence it has been used to identify and delineate high-temperature systems. In central-loop TEM soundings, current is induced by a time varying magnetic field generated by a current in a loop and the decaying induced magnetic field is monitored at the surface. For the MT method, the current in the ground is induced by the natural time varying electromagnetic field. MT soundings have the greatest penetration depth of all the electrical techniques.

2.1 Resistivity of rocks

Most rock-forming minerals are electrical insulators. Measured resistivities in the earth materials are primarily controlled by the movement of charged ions in pore fluids or by the conduction of secondary minerals. Although water itself is not a good conductor of electricity, groundwater generally contains dissolved compounds that greatly enhance its ability to conduct electricity. Hence, connected porosity and fluid saturation tend to dominate electrical resistivity measurements. In addition to pores, fractures within crystalline rock can lead to low resistivities if they are filled with fluids.

The resistivity of a material is defined as the resistance in ohms (Ω) between the opposite faces of a unit cube of the material (Kearey and Brooks, 1994). For a conducting cylinder of resistance (R), length (L) and cross-sectional area (A) the specific electrical resistance (often shortened by resistivity) is given by:

$$\rho = \frac{RA}{L} \tag{1}$$

where ρ = Specific resistivity (Ωm);
R = Resistance (Ω);
A = Area (m^2);
L = Length (m)

The electrical resistivity of rocks is influenced mainly by the following parameters (Hersir and Björnsson, 1991):

- Salinity of water;
- Temperature;
- Pressure;
- Porosity and permeability of the rock;
- Amount of water (saturation);
- Water-rock interaction and alteration.

2.1.1 Salinity of water

The bulk resistivity of a rock is mainly controlled by the resistivity of the pore fluid which is dependent on the salinity of the fluid. An increase in the amount of dissolved solids in the pore fluid can increase the conductivity by large amounts (Figure 3). Conduction in solutions is largely a function of salinity and mobility of the ions present in the solution. Therefore, the conductivity σ, of a solution may be determined by considering the current flow through a cross-sectional area of $1m^2$ at a voltage gradient of 1 V/m. This is expressed in Equation 2 (Hersir and Björnsson, 1991):

$$\sigma = \frac{1}{\rho} = F(c_1 q_1 m_1 + c_2 q_2 m_2 + \cdots) \qquad (2)$$

where σ = Conductivity (S/m);
F = Faraday's number (9.65×10^4 C);
c_i = Concentration of ions;
q_i = Valence of ions;
m_i = Mobility of ions.

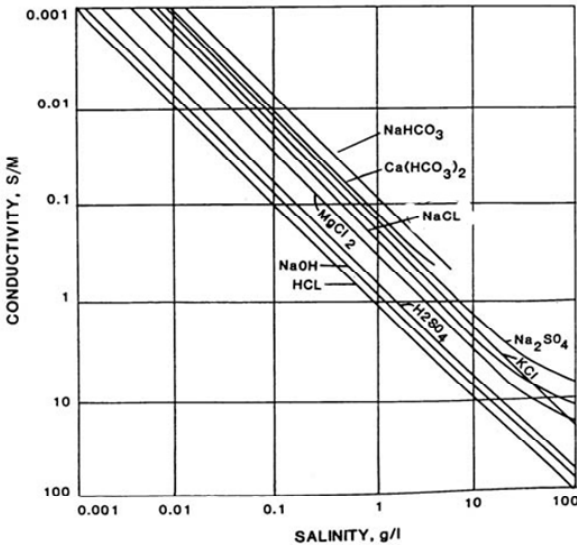

FIGURE 3: Pore fluid conductivity vs. salinity for a variety of electrolytes (from Keller and Frischknecht, 1966)

2.1.2 Temperature

At moderate temperatures, 0-200°C, resistivity of aqueous solutions decreases with increasing temperature (Figure 4). This is due to an increase in ion mobility caused by a decrease in the viscosity of the water. Dakhnov (1962) has described this relationship as:

$$\rho_w = \frac{\rho_{w_0}}{1 + \alpha(T - T_0)} \qquad (3)$$

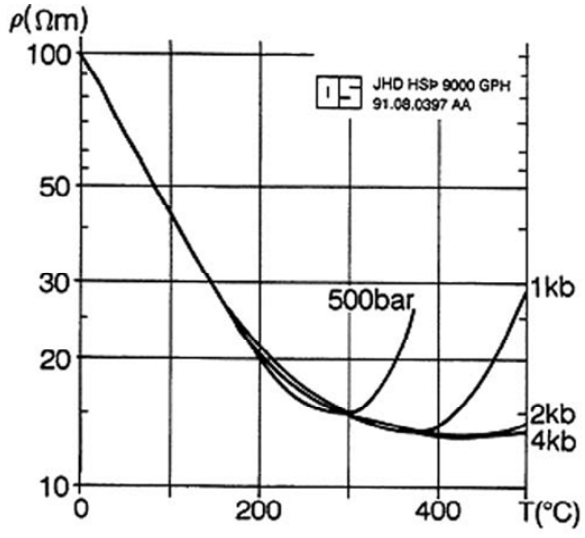

FIGURE 4: Electrical resistivity of water as a function of temperature at different pressures (Hersir and Björnsson, 1991)

where ρ_w = Resistivity of the fluid at temperature T (Ωm);
ρ_{wo} = Resistivity of the fluid at temperature T_o (Ωm);
α = Temperature coefficient of resistivity (°C), $\alpha \approx 0.023$°C;
T_0 = 23°C (room temperature).

At high temperatures, there is a decrease in dielectric permittivity of water, resulting in a decrease in the number of dissociated ions in solution. This effectively increases fluid resistivity. At temperatures about 300°C, fluid resistivity starts to increase as shown in Figure 4 (Quist and Marshall, 1968).

2.1.3 Porosity and permeability of the rock

Porosity is a measure of the void spaces in a material, and is measured as a fraction, between

0–1, or as a percentage from 0–100%. More specifically, porosity of a rock is a measure of its ability to hold fluid. Permeability, on the other hand, is a measure of the ability for fluid flow through a rock. Both porosity and permeability are important for electrical conductivity of rocks.

It has been observed that resistivity varies approximately as inverse powers of the porosity when the rock is fully saturated with water (Keller and Frischknecht, 1966). This observation has led to the wide spread use of an empirical function relating resistivity and porosity known as Archie´s law given by the formula:

$$\rho = a\rho_w \varphi^{-m} \quad (4)$$

where ρ = Bulk resistivity
ρ_w = Resistivity of the pore fluid
φ = Interconnected porosity expressed as a fraction per unit volume of rock
a = Empirical parameter varies from < 1 for inter-granular porosity to slightly above 1 for rocks with joint porosity;
m = Cementing factor, usually about 2

Permeability is a measure of how well fluids will flow through material. Effects, like the packing, shape and sorting of granular materials, control the rock's permeability. Although a rock may be highly porous, if the voids are not interconnected, then fluids within the closed, isolated pores cannot move. The degree to which pores within the material are interconnected is known as effective porosity. Rocks such as pumice and shale can have high porosity, yet can be nearly impermeable due to the poorly interconnected voids. The range of values for permeability in geological materials is extremely large. The most permeable materials have permeability values that are millions of times greater than the least permeable. Permeability is often directional in nature. Secondary porosity features, like fractures, frequently have a significant impact on the permeability of the material. In addition to the characteristics of the host material, the viscosity and pressure of the fluid also affect the rate at which the fluid will flow (Lee et al., 2006).

2.1.4 Water-rock interaction and alteration

Geothermal water reacts with rock to form secondary alteration minerals. The distribution of alteration minerals provides information on the temperature of the geothermal system and the flow path of the geothermal water. The alteration mineralogy provides information on the physicochemical characteristics of the geothermal water. The alteration intensity is normally low for temperatures below 50-100°C. At temperatures lower than 220°C, low-temperature zeolites and the clay mineral smectite are formed (Árnason et al., 2000). The range where low-temperature zeolites and smectite are abundant is called the smectite-zeolite zone. In the temperature range from 220 to about 240-250°C, the low-temperature zeolites disappear and the smectite is transformed into chlorite in a transition zone, the so-called mixed-layer clay zone, where smectite and chlorite coexist in a mixture. At about 250°C the smectite has disappeared and chlorite is the dominant mineral, marking the beginning of the chlorite zone. At still higher temperatures, about 260-270°C, epidote becomes abundant in the so-called chlorite-epidote zone. This zoning applies for fresh water basaltic systems. In brine systems, the zoning is similar but the mixed-layer clay zone extends over a wider temperature range, or up to temperatures near 300°C (Árnason et al., 2000).

Normally one would expect the resistivity of a geothermal system to decrease with increasing temperature. However, in high-temperature volcanic areas the resistivity in the chlorite and chlorite-epidote alteration zone, increases .due to an extremely low concentration of mobile cations. Figure 5 demonstrates the relationships between resistivity, alteration and temperature both for saline and fresh water systems. At depths, where the resistivity increases below a low-resistivity zone, a chlorite alteration zone is expected, indicating a temperature of 250°C or higher, provided the alteration is in equilibrium with the temperature. If the geothermal system has cooled down, then the alteration

remains the same and hence the resistivity structure is the same. In such a case the interpretation of the resistivity structure can be misleading since it reflects alteration minerals that were formed in the past.

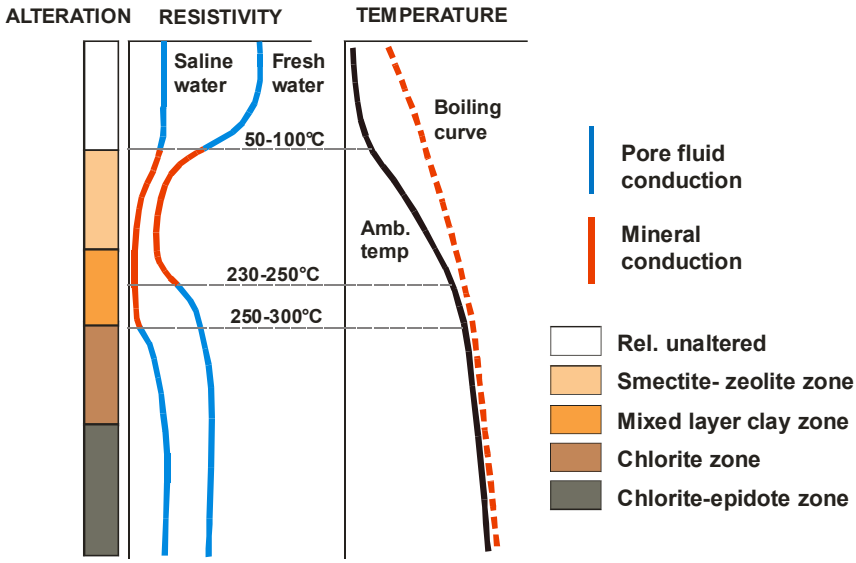

FIGURE 5: General resistivity structure of a high-temperature geothermal system showing resistivity variation with alteration and temperature (modified from Árnason et al., 2000)

3. THE TRANSIENT ELECTROMAGNETIC (TEM) METHOD

3.1 TEM theory

In the central loop TEM method a constant current is transmitted in a square loop of wire placed on the ground generating a static primary magnetic field around it. The current is then turned off abruptly and the decaying magnetic field induces currents in the ground. These currents decrease, due to Ohmic losses, and the secondary magnetic field decays with time. Figure 6 shows a schematic field layout and Figure 7 the current waveform and the induced voltage in the receiver coil. Just after the transmitter is switched off, the secondary magnetic field from the current in the ground will be equivalent to the primary magnetic field (which is no longer there) but with time it will diffuse downwards and outwards resulting in increasing depth of penetration with time (Figure 6). The magnitude and rate of decay of the secondary magnetic field is monitored by measuring the voltage induced in a receiver coil usually placed at the centre of the transmitter loop, as a function of time after the transmitter current is turned off. The current distribution and the decay rate of the secondary magnetic field depend on the resistivity structure of the earth with the decay being more gradual over a more conductive earth (Árnason, 1989).

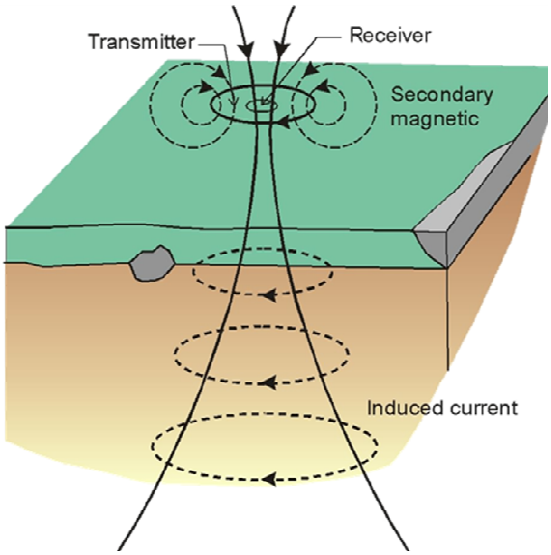

FIGURE 6: The central loop TEM configuration (from Hersir and Björnsson, 1991)

The depth of penetration in the central loop TEM-sounding is dependent on how long the induction in the receiver coil can be traced before it is drowned in noise. At so-called late times (described later), the induced voltage in the receiving coil on a homogeneous half space of conductivity, σ is (Árnason, 1989):

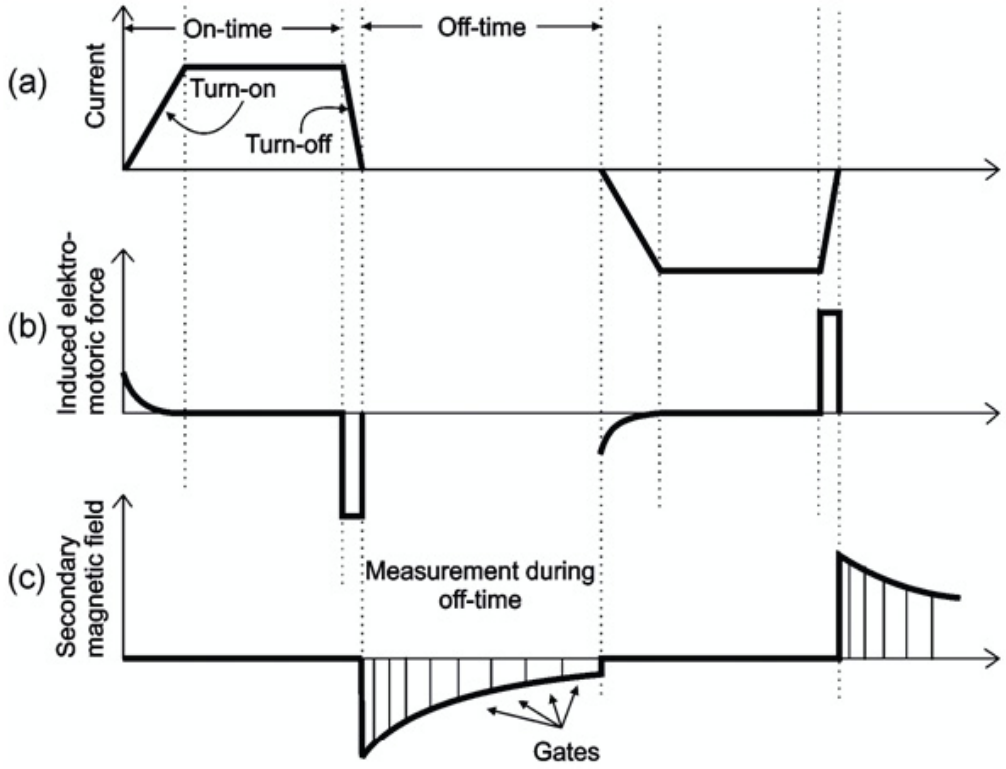

FIGURE 7: Basic principles of the TEM method: (a) The current in the transmitter loop; (b) The induced electromotive force in the ground; and (c) The secondary magnetic field measured in the receiver coil (from Christensen et al., 2006)

$$V(t,r) \approx I_0 \frac{C(\mu_0 \sigma r^2)^{3/2}}{10\pi^{1/2}\, t^{5/2}} \tag{5}$$

where $C = A_r n_r A_s n_s \dfrac{\mu_0}{2\pi r^3}$

and
n_r = Number of turns on the receiver coil;
A_r = Area of the receiver coil [m^2];
A_s = Area of the transmitting loop [m^2];
n_s = Number of turns in transmitter loop;
t = Time elapsed after the current in the transmitter is turned off [s];
μ_0 = Magnetic permeability [Henry/m];
$V(t,r)$ = Transient voltage [V];
r = Radius of the transmitter loop [m];
I_0 = Current in the transmitting loop [A].

This shows that the transient voltage for late times, after the current in the transmitter is abruptly turned off, is proportional to $\sigma^{3/2}$ and falls off with time as $t^{-5/2}$. This leads to the definition of the late time apparent resistivity by solving for the resistivity in Equation 5 leading to Equation 6:

$$\rho_a = \frac{\mu_0}{4\pi}\left[\frac{2I_0\mu_0 A_r n_r A_s n_s}{5t^{5/2}V(t,r)}\right]^{2/3} \tag{6}$$

3.2 Homogenous earth

The time-behaviour of the diffusing current is divided into three phases according to their characteristics as illustrated in Figure 8 which shows induced voltage as a function of time for a homogeneous earth. In the early phase the induced voltage is constant in time. In the intermediate phase, the voltage starts to decrease with time and with steadily increasing negative slope on a log-log scale until the late time phase is reached where the voltage response decreases with time in such a way that the logarithm of the induced voltage decreases linearly as a function of the logarithm of time. The slope of the response curve in the late phase is -5/2 in accordance with Equation 5 which is only valid for the late-time phase.

Figure 9 shows that the apparent resistivity at early time increases with decreasing resistivity of the half space and also that the transitions from early to late time get shifted towards earlier times as the resistivity of the half space increases. However, it should be noted that the response curve has the same shape for the different half space resistivities. When the apparent resistivity for a homogenous half-space is plotted as a function of time, it approaches asymptotically the true resistivity of the half-space for late times, as can be seen in Figure 9.

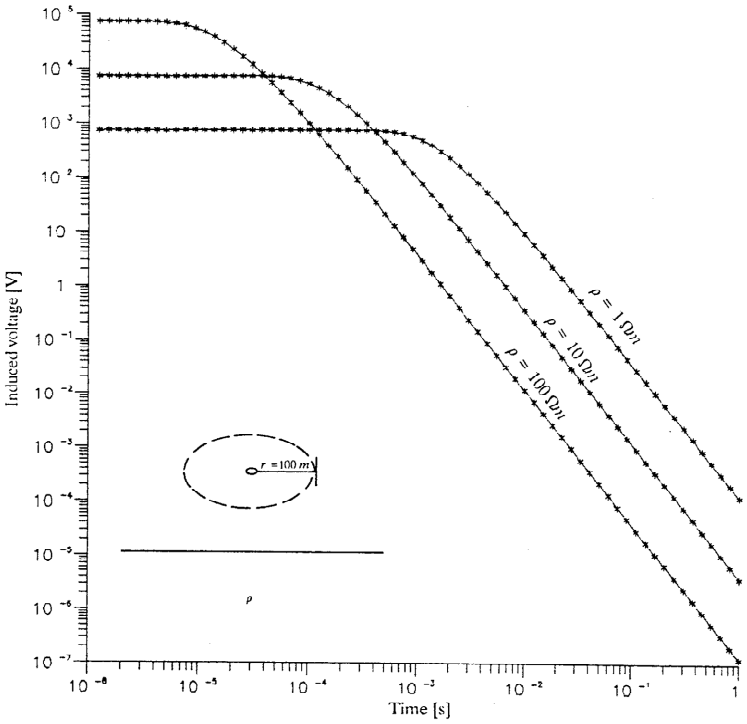

FIGURE 8: Voltage response for homogenous half space of 1, 10, and 100 Ωm (from Árnason, 1989)

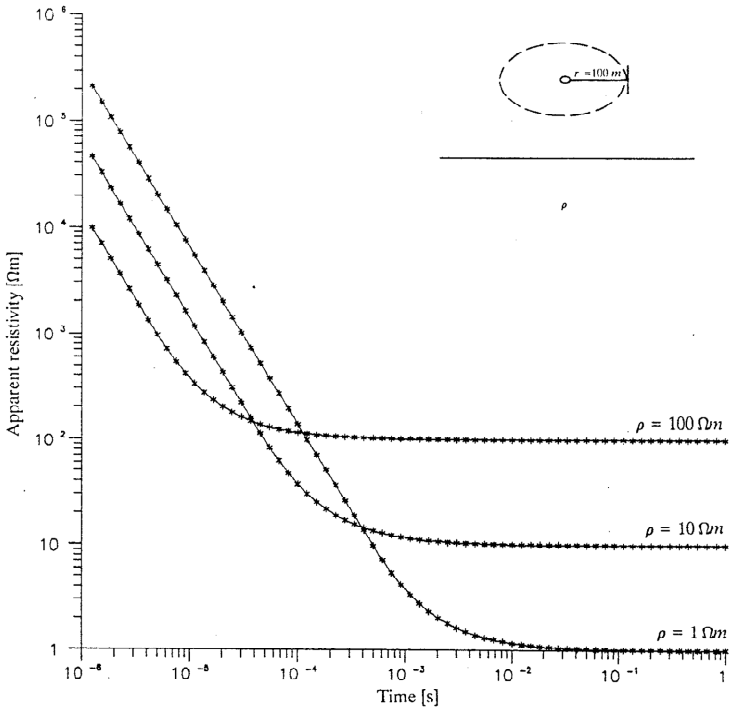

FIGURE 9: Late time apparent resistivity for homogenous half space of 1, 10 and 100 Ωm (from Árnason, 1989)

4. THE MAGNETO-TELLURIC (MT) RESISTIVITY METHOD

4.1 Basic theory

MT is an electromagnetic geophysical method to image the earth's subsurface resistivity structure. Natural variations in the earth's magnetic field induce electric currents (or telluric currents) in the ground which depend on the Earth's resistivity. Both magnetic and electric fields are measured on the earth's surface in two orthogonal directions. The ratio of the electric field and the magnetic field (impedance tensor) holds information about the subsurface conductivity. The high frequency gives information about the shallow subsurface while the low frequency provides information about the deeper structures.

At frequencies higher than 1 Hz, the magnetic source originates from lightning discharges in the equatorial belt while the low frequencies <1 Hz originate from the interaction between the solar wind and the earth's magnetic field. These natural phenomena create MT source signals over the entire frequency spectrum (generally 10 kHz to few thousand seconds).

The MT method can explore down to hundreds of kilometres, which makes it the EM method which has the most exploration depth of all the EM methods, and is practically the only method for studying resistivity deeper than a few kilometres. The depth of penetration of electromagnetic fields within the earth depends on the period and the earth's conductivity structure. The propagation of EM fields is described by the following set of relationships, called the Maxwell equation which holds true for all frequencies:

Faraday's law

$$\nabla \times \mathbf{E} = -\mu \frac{\partial H}{\partial t} \tag{7}$$

Ampéré's law

$$\nabla \times \mathbf{H} = \mathbf{J} + \varepsilon \frac{\partial E}{\partial t} \tag{8}$$

where **E** = Electrical field intensity (V/m);
H = Magnetic field intensity (A/m);
J = Electrical current density, and $\mathbf{J} = \sigma \mathbf{E}$;
σ = Conductivity (Siemens/m); $\rho = 1/\sigma$ (Ωm);
ε = Electrical permittivity;
μ = Magnetic permeability.

4.2 Electromagnetic induction in a homogenous earth

The ratio of electric to magnetic field intensity is a characteristic measure of the electromagnetic properties often called the characteristic impedance (Equations 9 and 10):

$$Z_{xy} = \frac{E_x}{H_y} = \frac{i\omega\mu_0}{k} \tag{9}$$

$$Z_{yx} = \frac{E_y}{H_x} = -\frac{i\omega\mu_0}{k} \tag{10}$$

where Z_{xy}, Z_{yx} = Characteristic impedance in x and y directions;
ω = Angular frequency ($2\pi f$) where f is frequency (Hz);
μ_0 = Magnetic permeability (H/m);
$E_{x,y}$ = Electric field intensity (V/m) in x, y direction;

$H_{x,y}$ = Magnetic field intensity (Tesla) in x, y direction;
k = $\sqrt{i\omega\mu(i\omega\varepsilon + \sigma)}$ stands for the wave propagation constant;
ε = Dielectric permittivity (C/Vm);
σ = Electric conductivity.

The term $\omega\varepsilon$ in wave propagation constant k is much smaller than conductivity σ and can be ignored, therefore, $k = \sqrt{i\omega\sigma}$. Putting this into Equations 9 and 10, gives:

$$Z_{xy} = \frac{E_x}{H_y} = \frac{i\omega\mu}{k} \approx \frac{i\omega\mu}{\sqrt{i\omega\sigma}} = \sqrt{i}\sqrt{\omega\rho\mu} = \sqrt{\omega\mu\rho}\,.\, e^{i\pi/4} \quad (11)$$

$$Z_{yx} = \frac{E_y}{H_x} = -\frac{i\omega\mu}{k} = -Z_{xy} \quad (12)$$

The phase angle by which H_y lags E_x is π/4 as explained in Figure 10. If the earth is homogenous and isotropic, then the true resistivity of the earth is related to the characteristic impedance through the following relationship (e.g. Hermance, 1973):

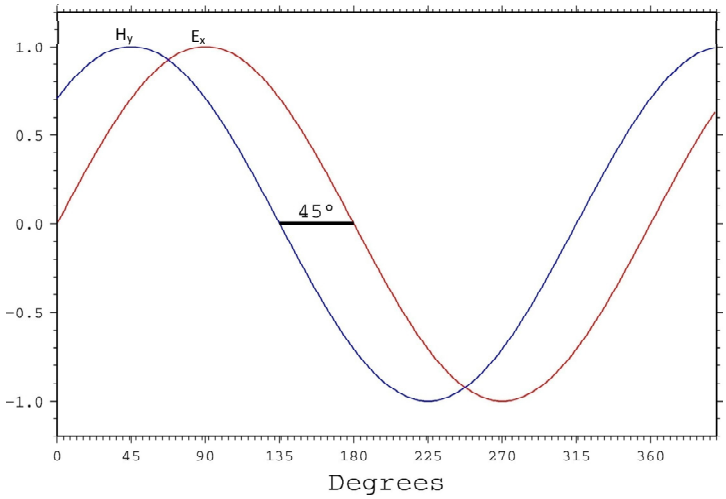

FIGURE 10: Homogenous half space response of electric and magnetic field describing the 45° phase difference of the E and H fields; their amplitudes are not the same

$$\rho = \frac{1}{\mu\omega}\left|Z_{xy}\right|^2 = \frac{1}{\mu\omega}\left|Z_{yx}\right|^2 \quad (13)$$

For a non-homogeneous earth the apparent resistivity (ρ_a) can be defined as if the earth were homogeneous using this same formula.

In practical units for homogeneous earth the resistivity, ρ, in the above equation can be written as:

$$\rho_a = 0.2T|Z|^2 = 0.2T\left|\frac{E_x}{B_y}\right|^2 \quad (14)$$

where θ is the phase angle = arg(Z) = π/4 or 45°;
E' is the electrical field (mV/km); $E' = E\times10^{-6}$,
B' is the magnetic field (nT); $B' = B\times10^{-9;}$ where B=, =μH is the magnetic field in Tesla, and $\mu=4\pi\times10^{-7}$.

For a non-homogeneous earth the apparent resistivity (ρ_a) and phase (θ_a) are functions of frequency and are defined as follows:

$$\rho_a = 0.2T|Z_0|^2 \text{ and } \theta_a = \arg(Z_0) \neq 45^0 \quad (15)$$

4.2.1 Skin depth

The skin depth, δ is the depth where the electromagnetic fields have been reduced to e^{-1} of its original value at the surface. The propagation is time dependent on the oscillating electromagnetic fields, that is **H**, **E** ~ $e^{i\omega t}$ and is a vertically incident plane wave. Therefore, skin depth is used as a scale length for the time-varying field, or an estimate of how deep such a wave penetrates into the earth, and is given by:

$$\delta = \frac{1}{Real(k)} = \frac{1}{Real\ (i\omega\mu\sigma)} = \sqrt{\frac{2}{\omega\mu\sigma}} = \sqrt{\frac{2T\rho}{2\pi \times 4\pi \times 10^{-7}}} = \frac{10^3}{\pi} \times \sqrt{{}^{20}/_{8}} \times \sqrt{T\rho} \qquad (16)$$

or

$$\delta \approx 500\sqrt{T\rho} \qquad (16a)$$

where δ = Skin depth (m);
T = Period (s);
ρ = Resistivity (Ωm).

4.3 MT dead band

MT data acquisition is prone to a number of problems one of them being the dead band problem. This occurs in the frequency band between 0.1 and 10 Hz in which natural signals are typically weak with the minimum at around 1 Hz. This problem is attributable to the inductive source mechanisms, one effective below ~1 Hz and the other above ~1 Hz, which causes a reduction in data quality. Noise due to wind is also typically highest in this frequency range thus still diminishing the signal to noise ratio in the frequency band

5. RESISTIVITY STUDY OF OLKARIA DOMES GEOTHERMAL FIELD

5.1 TEM survey and instrumentation

In this study a total of 52 central loop TEM soundings were carried out in the Domes area spread over about 45 km^2. The stations are scattered within the prospect area with denser coverage in the areas where wells have been drilled. The locations of the soundings are shown in Figure 11.

The TEM equipment used is from Zonge and consists of a current transmitter, XMT transmitter controller, GDP-16 data logger, a receiver coil with an effective area of 10,000 m^2, a 120 VA power generator, a voltage regulator and a transmitter loop. Before data acquisition, both the receiver and the transmitter controller high-precision crystals are warmed up for a period of about an hour and then synchronized to ensure that induced voltage is measured by the receiver at the correct time after the current turn-off. In the field setup a 300 m × 300 m transmitter wire loop was used and a 9 A half-duty square wave current was transmitted at frequencies 16, 8, 4 and 2 Hz. The transient signal was recorded in the time interval of 36.14 μsec to 96.85 msec at logarithmically spaced sampling gates after the current turn-off. For each frequency several repeated transients were stacked and stored in a memory cache inside the Zonge data logger and later transferred to a personal computer for processing.

5.2 TEM data processing and 1-D interpretation

The raw TEM data was processed by the program TemZ, a modified version of Temx, to handle the Zonge data (Árnason, 2006). This program averages data acquired at the same frequency and calculates late time apparent resistivity as a function of turn-off time. It also enables visual editing of raw data to remove outliers and unreliable data points before the data can be used for interpretation.

The 1-D inversion of TEM was achieved by software called TEMTD, a UNIX program (developed at Icelandic Geosurvey by Knutur Árnason,). This software assumes that the source loop is a circular source field and that the receiver coil/loop is at the centre of the source loop. For practice reasons, a

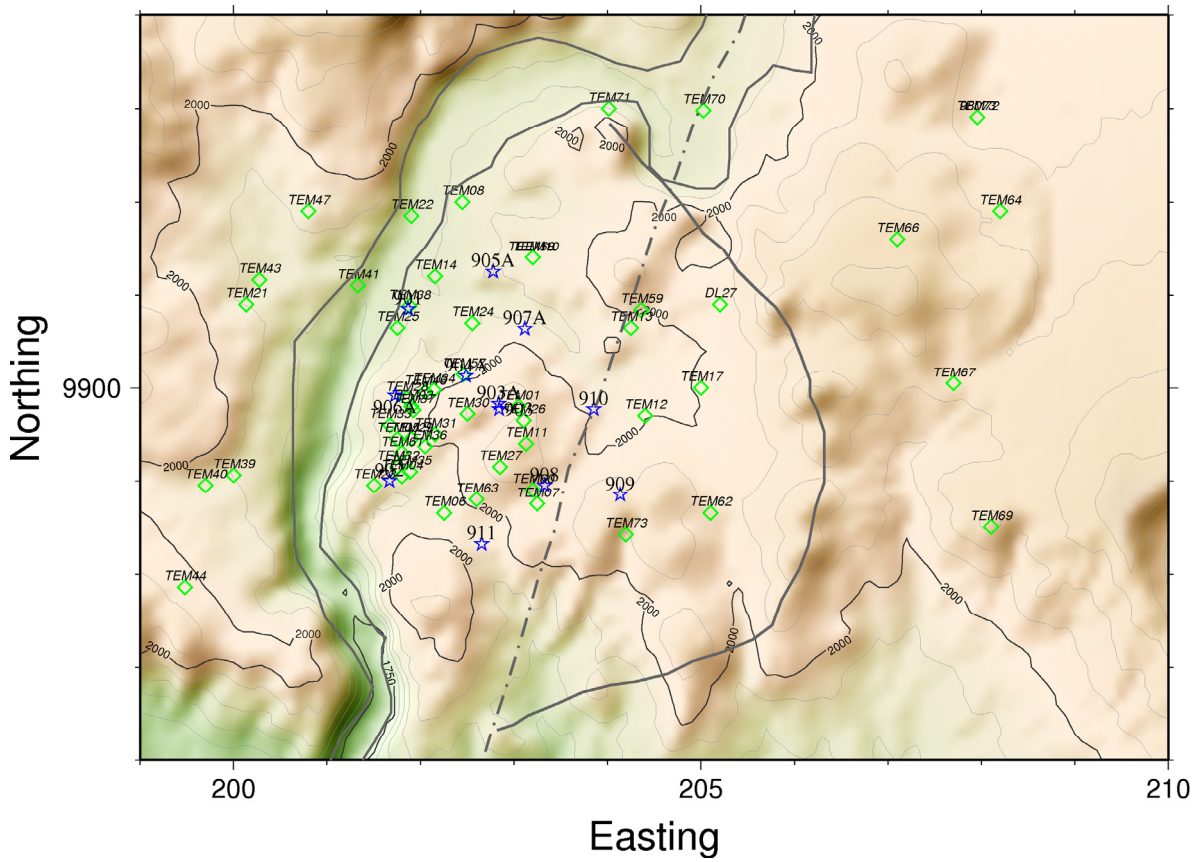

FIGURE 11: Location of TEM soundings (green diamonds); the topography data on the base map was downloaded from the internet; shown on the map is the Ol´Njorowa gorge to the west of Domes field, a NNE-SSW fault in the middle and the ring structure to the east; Easting and Northing are UTM coordinates in km using Arc 1960 datum, while the blue stars are location of boreholes

square loop is used with equal area to that of the circle. The current waveform is also assumed to have equal current-on and current-off time segments. The transient response is calculated both as induced voltage and late time apparent resistivity as a function of time. The inversion algorithm used in this program is the linear, damped, least-squares inversion (Árnason, 2006). The misfit function is the root-mean-square difference between measured and calculated values (chisq), weighted by the standard deviation of the measured values. In this study, the measured voltages were chosen for inversion.

All the TEM soundings in the Domes area were interpreted by 1-D (layered earth) inversion. The inversion was done by the Occam (minimum structure) inversion An example of an inversion result is shown in Figure 12. In 1-D inversion it is assumed that the earth consists of horizontal layers with different resistivity and thicknesses. The 1-D interpretation seeks to determine the layered model where the response best fits the measured responses. When interpreting TEM resistivity it must be born in mind that the depth of exploration of the TEM soundings is much greater in resistive earth than in conductive environments. This is because the fields die out faster in conductive materials than in a resistive one.

5.3 MT survey and instrumentation

The data was acquired using a 5-channel MT data acquisition system (MTU-5A) from Phoenix Geophysics. The instrumentation consisted of a data recorder, induction coils, non-polarizing

electrodes, Global Positioning System (GPS), 12 V battery, flash memory for data recording, and telluric and magnetic cables.

The layout is made such that the electric dipoles are aligned in magnetic North-South and East-West, respectively, with corresponding magnetic channels in orthogonal directions; the third channel is positioned vertically in the ground as demonstrated on Figure 13. Before data acquisition, a start-up file is prepared with parameters like gains, filters, time for data acquisition and calibrations for both equipment and the coils and stored on a flash disk in the equipment. The ground contact resistance is generally measured to gauge the electrode coupling to the ground and both a high pass filter and an anti-aliasing filter are used with a corner frequency of 0.005 Hz to remove the effect of self potential from the electric dipoles. The electric field was measured by lead chloride porous pots and the magnetic sensors were buried about 20 cm below the surface to minimize the wind effect.

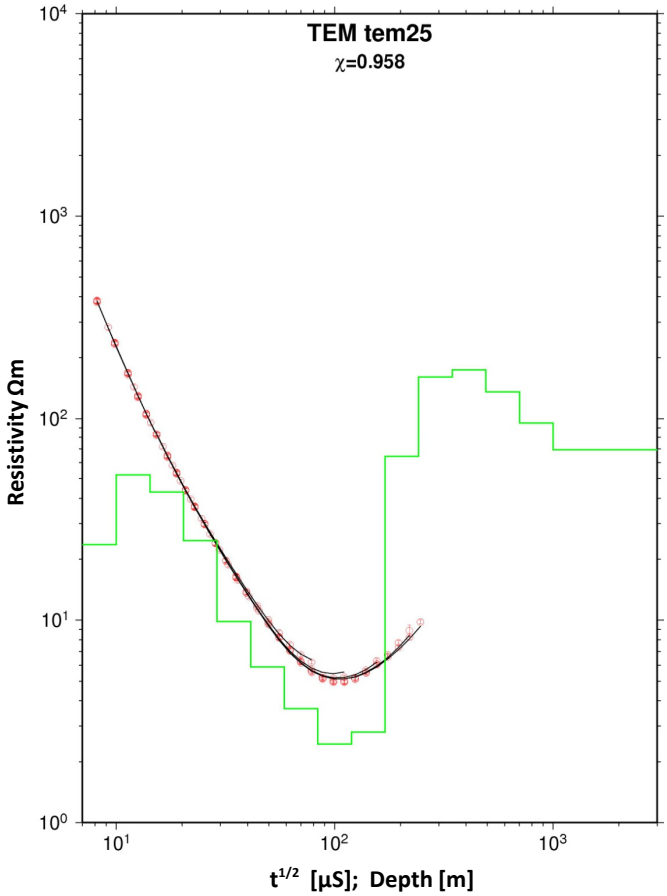

FIGURE 12: TEM sounding from the Domes area and its 1-D inversion illustrating the TEM apparent resistivity curve and its interpretation; the red (dark gray) dots are measured late-time apparent resistivities and the black solid line is the apparent resistivity calculated from the model shown with the step-like green (light gray) curve

MT data is acquired for about 20 hrs, giving the frequency range from 320 Hz and often up to few thousand seconds, which generally ensures investigation depths down to several tens of km. In this survey the long period data was not achieved at most of the stations because signals were drowned in noise at low frequencies. The penetration depth of the electromagnetic wave depends on the frequency where low frequency waves have greater depth of penetration than high-frequency waves. During data acquisition, one 5-component MT station was installed away from the field of focus and maintained as a remote reference station which was later used during data processing to reduce the effect of local cultural noise. This is based on the fact that a magnetic signal tends to be the same over a large area and that local disturbances at the local station may not be recorded at the remote station, i.e. the noise part is not coherent at the two sites. During robust processing, estimates

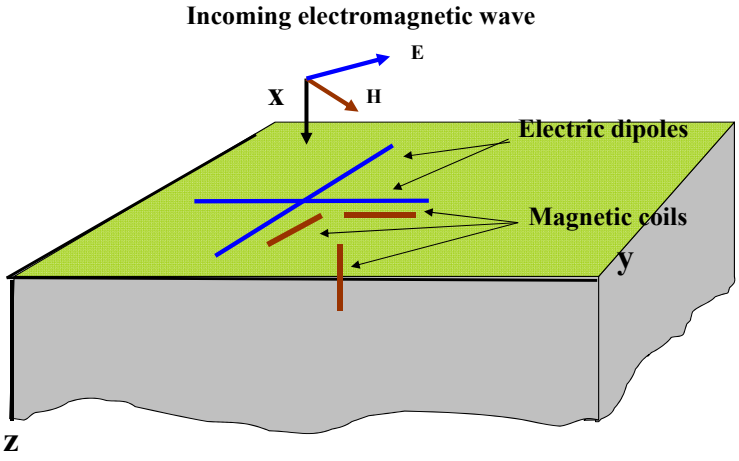

FIGURE 13: MT field layout

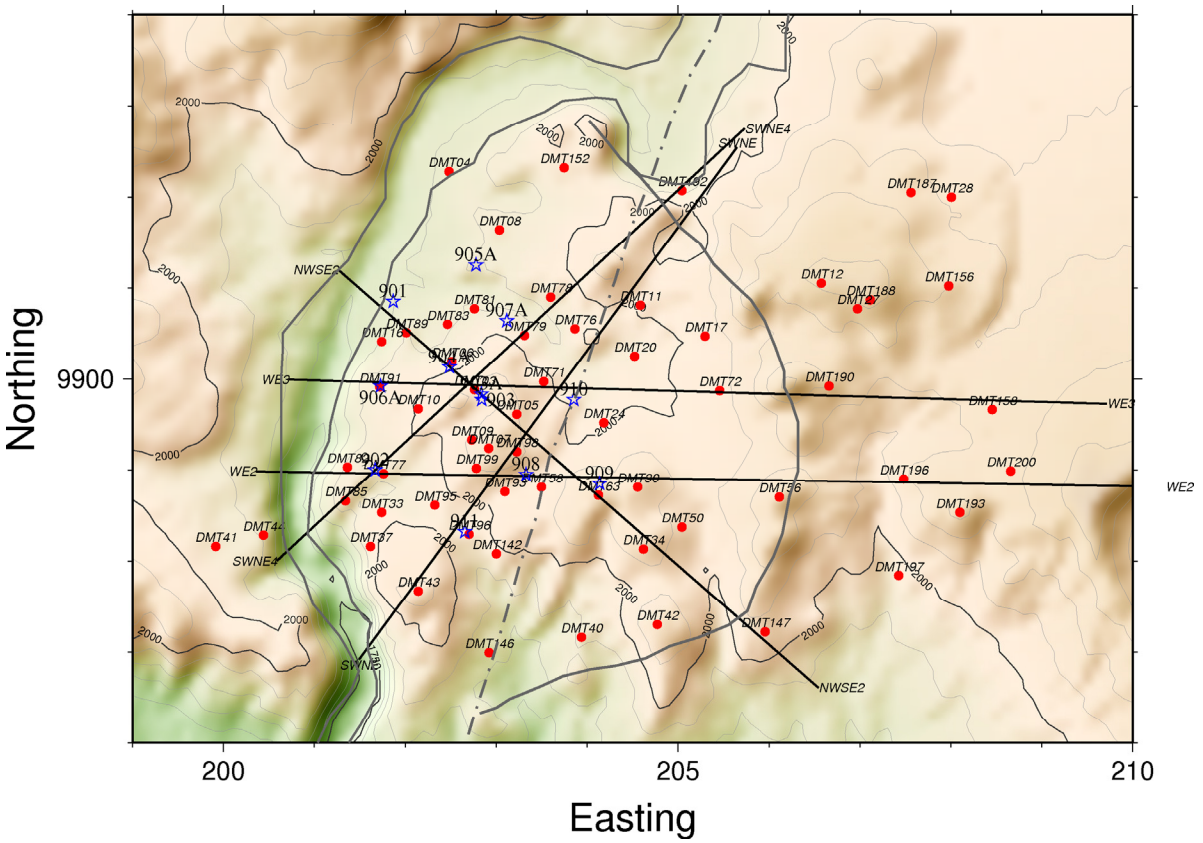

FIGURE 14: The MT soundings distribution (red dots) and the black thick lines are locations of resistivity cross-sections over the prospect area

of magnetotelluric and geomagnetic response functions are determined using the coherency and expected uniformity of the magnetic source field as quality criteria.

All the stations were time synchronized via signals from Global Positioning System (GPS) satellites so that time-series data from the remote reference station was processed in combination with data acquired at the same time from the other stations to reduce the effects of local noise and improve the quality of the survey results.

A total of 70 MT soundings were considered for interpretation in the Olkaria Domes prospect covering an area of about 45 km^2 as can be seen in Figure 14.

5.4 MT data processing and interpretation

Time-series data downloaded from the MT equipment was processed by the SSMT2000 programme, provided by the equipment manufacturer, Phoenix Geophysics of Canada. First the parameter file was edited to reflect the data acquisition setup and then the resulting time-series data were then Fourier transformed to the frequency domain. The time series data were converted into frequency domain by using a cascade decimation method. From the Fourier transform band averaged cross- and auto-powers were calculated using the robust processing method. The cross-powers were then graphically edited by the MT editor program to remove the noisy data points and evaluate "smooth" curves for both phase and apparent resistivity. The final cross- and auto powers, as well as all relevant MT parameters calculated from them (impedances, apparent resistivity, phase coherences, strike directions etc.) were stored in industry-standard file format (EDI files).

5.5 The MT static shifts

The MT method suffers from the so called static shift problem. This phenomenon is caused by local resistivity inhomogeneities which disturb the electrical field. The main cause is the accumulation of charges at resistivity boundaries causing the electrical field not to be continuous close to this boundary. The static shift is expressed by scaling of the apparent resistivity by an unknown factor (shifted on log scale). This shift is independent of frequency, at least for those frequencies generally used in MT soundings (Jones, 1988). The static shifts can be a big problem in volcanic environments where resistivity variations close to the surface are often extreme. These parallel shifts in an apparent resistivity curve can lead to large errors in inverted data. For instance, a shift down by S = 0.1 will, in interpretation, result in ten times too low resistivity values and about three times too small depths to resistivity boundaries (Árnason, 2008).

Several methods have been advanced as possible solutions for the static shift problem in MT. DeGroot-Hedlin (1991) and Ogawa and Ushida (1996) have proposed use of an inversion algorithm on MT data themselves to correct for static shift; this assumes that the shift multipliers are random and that the product of the shift multipliers is close to one for many soundings. This may not necessarily be correct, as seen in the variation of the shift values in the Domes field as shown in Figure 15. Another theory and the one that has been used in this report is the use of Central loop-induction TEM sounding to correct for static shift in MT data by jointly inverting both MT and TEM data. This is based on the fact that, for TEM measurements at late time there are no distortions due to near surface inhomogeneities since they do not involve measuring the electrical field. This has been tested by model calculations (e.g. Sternberg et al., 1988) and shown to be a useful method to correct for static shifts in MT soundings, at least for a 1-D resistivity environment.

The TEM apparent resistivity used to estimate the shift parameter in the MT data does not necessarily agree with either of the principle apparent resistivities (xy or yx) as shown in Figure 15. It may occur in between them, below them or agree with either of them. It should also be noted that the phase is not affected by the static shift problem.

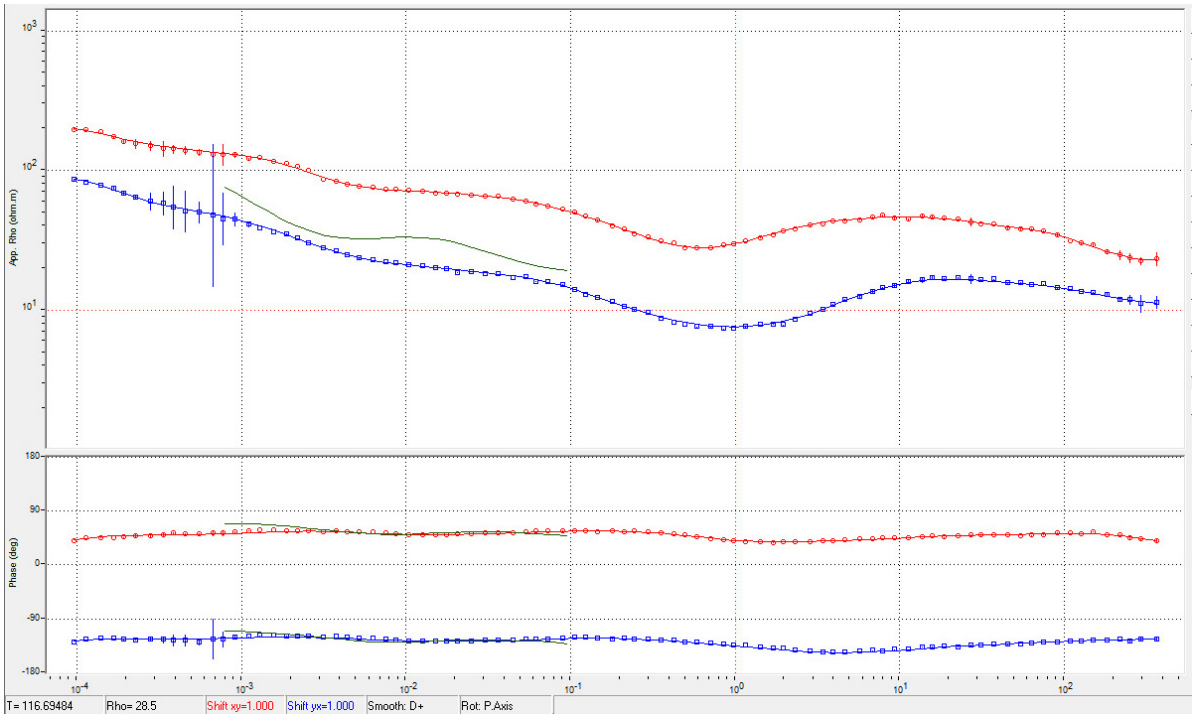

FIGURE 15: Static shift problem in MT apparent resistivity data; the red (dark gray) curve represents the apparent resistivity (upper frame) and phase (lower frame) in XY direction, the blue (gray) curve represents apparent resistivity in YX direction and the short green (gray) curve is the TEM response

5.6 Static shift analysis of MT data in Domes

Static shift analysis of the 62 MT soundings in the Domes area was done using the TEMTD joint inversion code and inverting for the rotational invariant determinant apparent resistivity and phase data. The shift factors are in the range of 0.2-2.1. This outcome indicates that about 57% of all the MT determinants apparent resistivity were shifted down whereas 23% were shifted up with only 20% not showing any static shift (Figure 16). Therefore, if interpretation was done without the static shift correction, then we would have an error of 80% in resolving the resistivity structure for this field.

Figure 17 shows the spatial distribution of the shift multipliers in the Domes area. The map shows that there are large areas where the MT apparent resistivity is consistently shifted downwards and other areas where it is shifted upwards.

In conclusion, it has been found out that correction for static shift by use of controlled-source EM sounding in a joint inversion with MT data can be very effective in providing a more accurate picture of the resistivity structure of the earth.

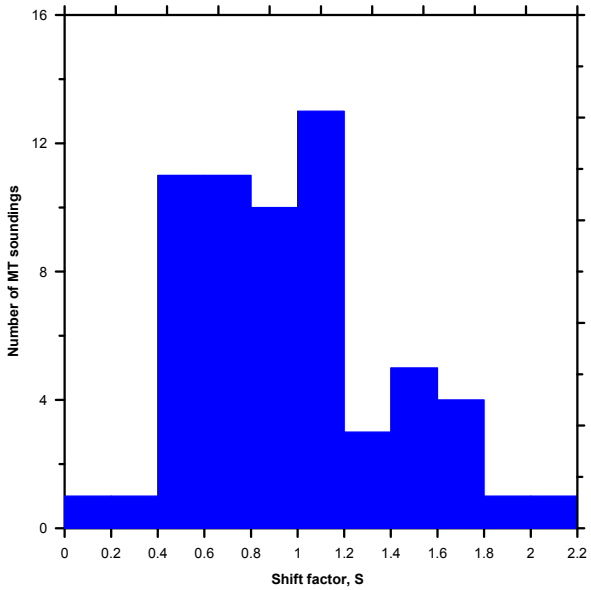

FIGURE 16: Histogram of static shift parameters for determining apparent resistivity in the Domes area

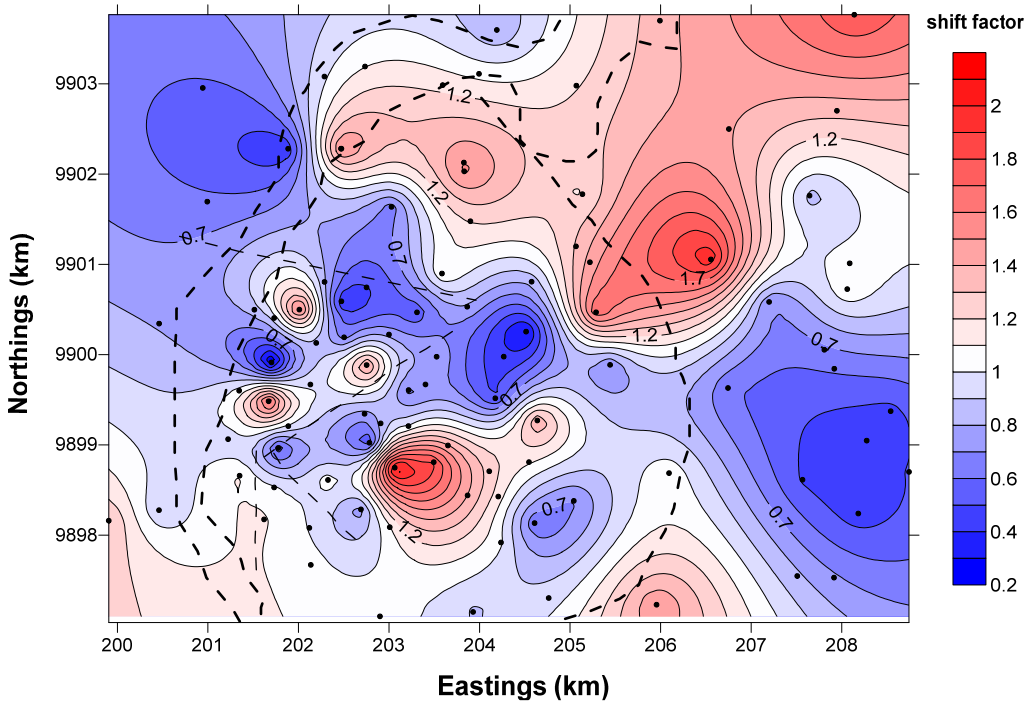

FIGURE 17: Spatial distribution of static shift parameters for determining apparent resistivity in the Domes area; the dotted lines represent the gorge, the ring structure and the faults within the study area, and the dots are the locations of MT stations

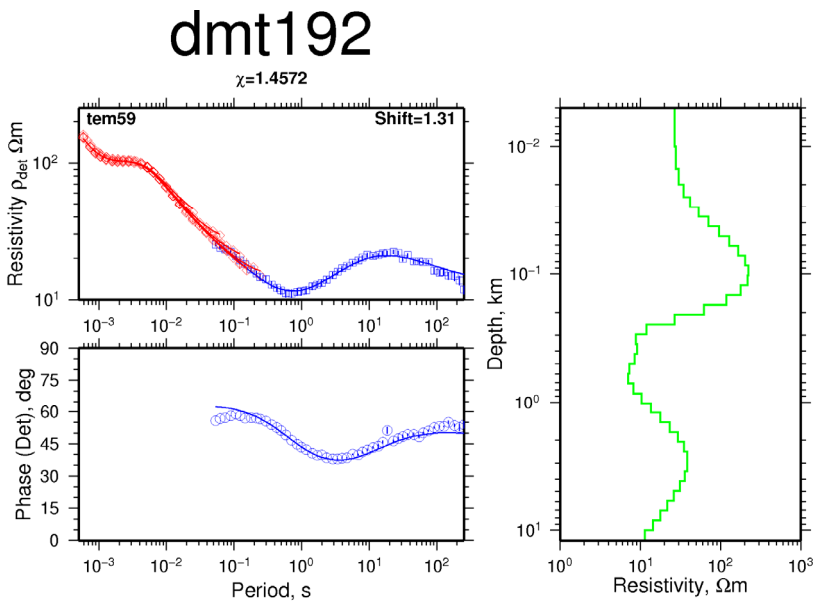

FIGURE 18: Typical result of a joint 1-D inversion of TEM and MT soundings; the red (dark) diamonds are measured TEM apparent resistivities and blue (gray) squares are the MT apparent resistivities and phase. Solid lines show the response of the resistivity model to the right. The shift multiplier is shown in the upper right hand corner of the apparent resistivity panel

6. JOINT 1-D INVERSION OF TEM AND MT SOUNDINGS

The TEMTD program does 1-D inversion of TEM and MT data separately or jointly. In this study the software was used to invert MT apparent resistivity and phase derived from the rotationally invariant determinant of the MT tensor elements. In the joint inversion, one additional parameter was also inverted for, namely a static shift multiplier needed to fit both the TEM and MT data with the response of the same model. The programme can do both standard layered inversion (inverting resistivity values and layer thicknesses) and Occam's (minimum structure) inversion with exponentially increasing layer thicknesses with depth. It offers a user specified damping of the first (sharp steps) and second order derivatives (oscillations) of model parameters (logarithm of resistivity and layer thicknesses) (Árnason, 2006).

An example of a 1-D joint inversion of MT and TEM data is shown in Figure 18, where the red (dark) diamonds are measured TEM apparent resistivities and the blue (gray) squares are the MT apparent resistivities and phase. Solid lines show the response of the resistivity model, shown to the right. The shift multiplier is shown in the upper right hand corner of the apparent resistivity plot. The TEM data has been converted from the time scale to the frequency scale according the the method suggested by Sternberg (1988).

For MT sites, where no nearby TEM stations exist, the closest TEM site was used for static shift correction. This might compromise the resolution of the resistivity structure since the distance between an MT site and the closest TEM site can be more than 500 m.

The inversion results are shown by the following selected cross-sections and iso-resistivity maps. A complete set of all the iso-resistivity maps and cross sections is published in a special Appendix report (Lichoro, 2009) where the inversion results of each sounding are also shown.

6.1 Cross-sections

Resistivity cross-sections were plotted from results obtained from 1-D inversion by a program called TEMCROSS (Eysteinsson, 1998), also developed at ÍSOR – Iceland Geosurvey. The program calculates the best line between the selected sites on a profile, and plots resistivity isolines based on the 1-D model generated for each sounding. It is actually the logarithm of the resistivity that is contoured so the colour scale is exponential but numbers at contour lines are resistivity values. Several vertical cross-sections were made through the survey area and their locations are shown in Figure 14. The maximum depth of resolution for each site is estimated and stored in a special file called MAXDEPTH and used to clip the model accordingly.

Cross-section NWSE2 is shown in Figure 19, cutting through wells OW901, OW904, OW903, OW908A and OW909. A high-resistivity layer (> 100 Ωm) occurs close to the surface below some of the sites, overlaying a low-resistivity layer extending down from 0.5 to 1 km. This high resistivity could be reflecting unaltered rocks near the surface. The low resistivity (< 10 Ωm) here correlates well with the alteration clay minerals as seen in the wells close to the profile. Below the low-resistivity zone is high resistivity, close to 50 Ωm and increases to above 100 Ωm and stays relatively high in the chlorite and chlorite-epidote zones as evidenced from the alteration mineralogy in the drill holes.

Cross-section SWNE4 is shown in Figure 20, with wells OW902 and OW903 projected onto the section. The top layer of about 300 m exhibits high resistivity reflecting un-altered rock formation. Underlying the high resistivity is a continuous 1 km thick low-resistivity layer, of about 10 Ωm. This layer correlates fairly well with the smectite-zeolite alteration zone obtained from the well logs.

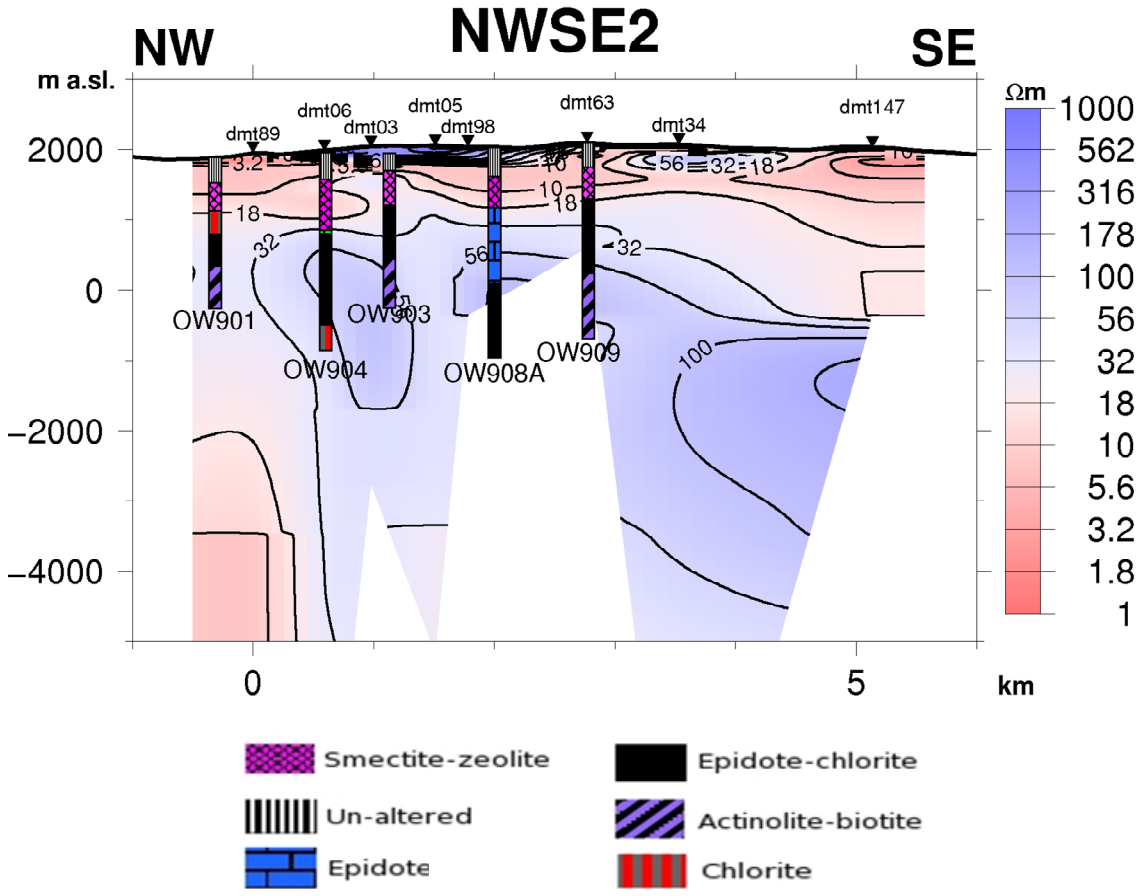

FIGURE 19: Resistivity cross-section NWSE2 according to joint 1-D inversion of TEM and MT data; the location is shown on the profile map in Figure 14. The vertical colour coded bars indicate alteration mineralogy from nearby wells projected on the profile

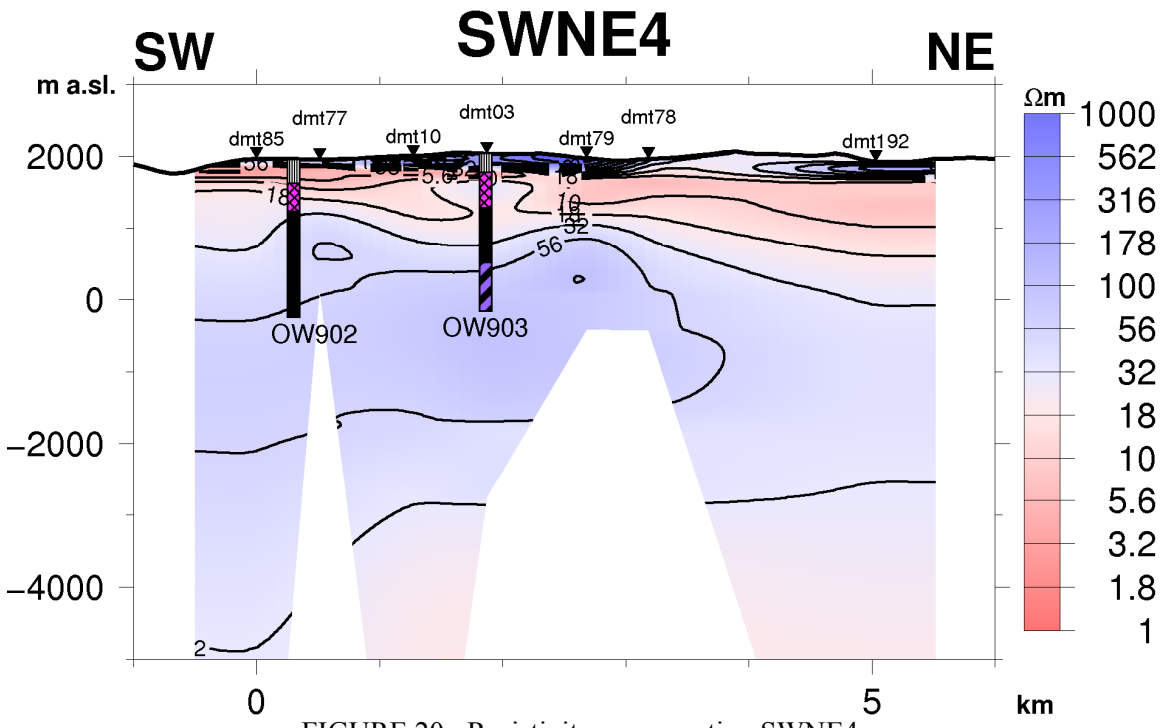

FIGURE 20: Resistivity cross-section SWNE4

Further below, the section presents a high-resistivity layer of > 50 Ωm which correlates with the chlorite-epidote high-temperature hydrothermal alteration zone. The low resistivity at 3-4 km below sea level is not well resolved due to the lack of long period data from sounding stations dmt79 and dmt78. Alteration zones in well OW902 correlate very well with the resistivity both in the smectite-zeolite zone and the chlorite-epidote zone but its reservoir temperature is not in agreement with alteration. This has been attributed to cooling in that part of the field indicating that the alteration is not in equilibrium with the present temperature.

Cross-section SWNE is shown in Figure 21. It shows a high-resistivity layer in the uppermost 300 m.

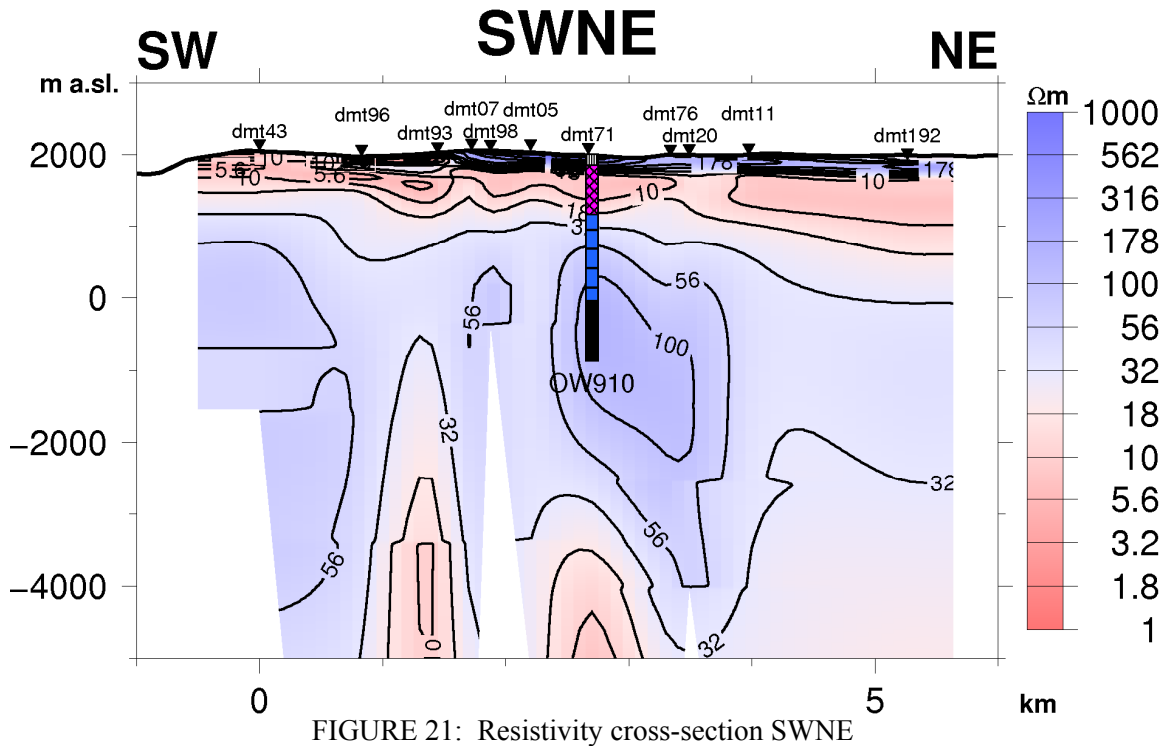

FIGURE 21: Resistivity cross-section SWNE

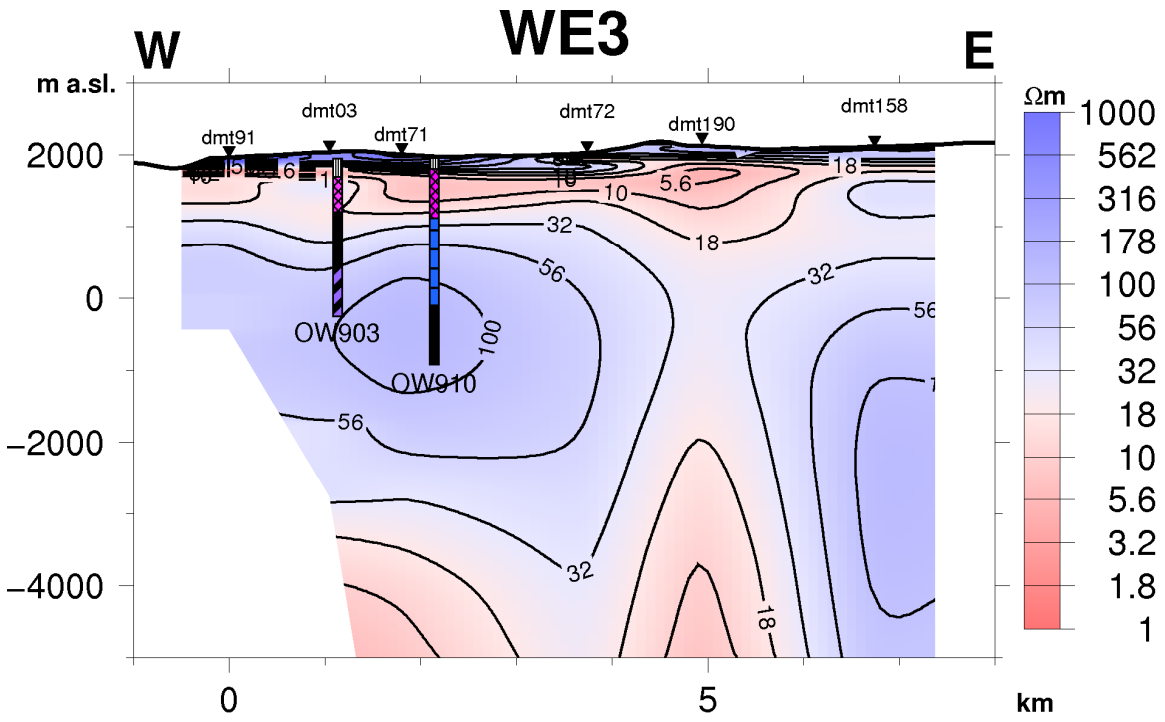

FIGURE 22: Resistivity cross-section WE3 according to joint 1-D inversion of TEM and determinant MT data

The uniform low-resistivity layer of about 10 Ωm correlates well with the smectite zone as seen in the alteration mineralogy of well OW910. Below the low-resistivity layer is a high-resistivity layer reaching 100 Ωm at about 2 km depth. To the southwest of well OW910 a lateral low-resistivity discontinuity can be seen protruding up to a depth of 1000 m b.s.l. below sounding dmt93. This low-resistivity anomaly could be reflecting a fault-like structure. Also below OW910 a low resistivity can be seen at about 6 km depth which could probably be related to the heat source for this part of the field.

Cross-section WE3 is shown in Figure 22. It presents a typical resistivity section expected in a high-temperature geothermal system, where at the top of a high-enthalpy geothermal system, a clay cap with expandable clay minerals is seen. Its resistivity is generally lower than in the overlying surface rocks. At depths of 4000 m b.s.l., a low resistivity is emerging below the wells; this is the same low resistivity seen in cross-section SWNE and could probably be the heat source for this field though it is not well resolved at depth. To the east of well OW910 and below sounding dmt190, low resistivity can be seen at depths of 4 km below the surface. This low-resistivity body could be a magmatic intrusion earlier inferred by seismic studies as an attenuating body below the ring structure (Simiyu et.al., 1998). This feature is not well resolved since the TEM sounding used for static shift correction is ~1km away from the MT site and, thus, could not represent the true shift. Beyond the ring of Domes another high-resistivity zone can be seen below sounding dmt158 down to several km depth.

Cross-section WE2 is shown in Figure 23, going through wells OW902, OW908A and OW909, and about 1 km south of cross-section WE3. A similar resistivity structure is presented here, with a high-resistivity top layer of un-altered sediments. Below is a low-resistivity layer (< 10 Ωm) reflecting the smectite-zeolite zone. At deeper levels is a high-resistivity layer with resistivity of 100 Ωm, correlating with the chlorite-epidote zone as seen in the wells and with the high temperatures greater than 300°C encountered in wells OW908A and OW909 at a depth of about 2 km. At a depth of 4 km below the surface beneath sounding dmt56 a low-resistivity layer is seen in section WE3, interpreted as a possible heat source. However, in this region the TEM soundings were a bit far (~ 1 km) from the MT stations and static shift correction might be wrong. The high resistivity below the low resistivity seen to the east of the ring structure in section WE3 is still prominent in this cross-section.

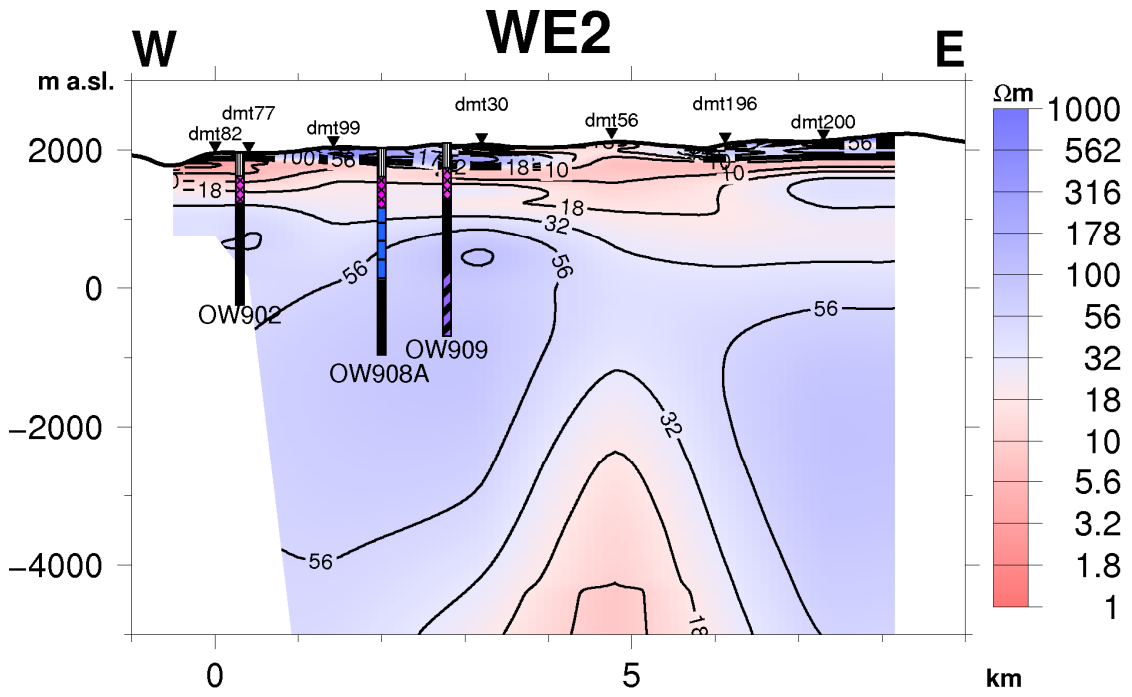

FIGURE 23: Resistivity cross-section WE2 according to joint 1-D inversion of TEM and determinant MT data

6.2 Iso-resistivity maps

Iso-resistivity maps were made by the TEMRESD programme, which generates iso-resistivity maps at different elevations from the 1-D Occam models (Eysteinsson, 1998). The resistivity is contoured and coloured in a logarithmic scale. The elevation of the Domes area is generally about 2100-2200 m a.s.l. In this report, iso-resistivity maps are presented from 1950 m a.s.l. down to 10,000 m b.s.l., with the upper iso-maps reflecting the TEM resistivity structures and the deeper ones representing the depth of penetration of the MT soundings. As in the cross-sections, soundings that have estimated depth of resolution that is shallower than the depth of the iso-resistivity map are not included in the generation of that map.

A resistivity map at 1950 m a.s.l. is shown in Figure 24. This elevation is generally between 50-250 m below the surface within the study area. The map shows high resistivity (100 – ~1000 Ωm) in the western and northern sectors of the study area; the high resistivity is probably due to un-altered formations that overlie the low-resistivity region. Low-resistivity anomalies are seen, one along the ring of Domes from the south and another in the middle of the study area in a NNE-SSW direction superimposed between high-resistivity zones.

A resistivity map at 1800 m a.s.l. is shown in Figure 25. This elevation is at about 400 m depth from the surface. The low-resistivity appears in the eastern and central parts with a linear low-resistivity (< 10 Ωm) anomaly aligning N-S in the eastern portion of the map. The low resistivity spreading over the area is associated with the alteration low-resistivity clay region overlaying the high-resistivity core of the geothermal system. The high-resistivity anomaly patches seen in the middle portion of the map are probably remnants of the un-altered zone at this depth.

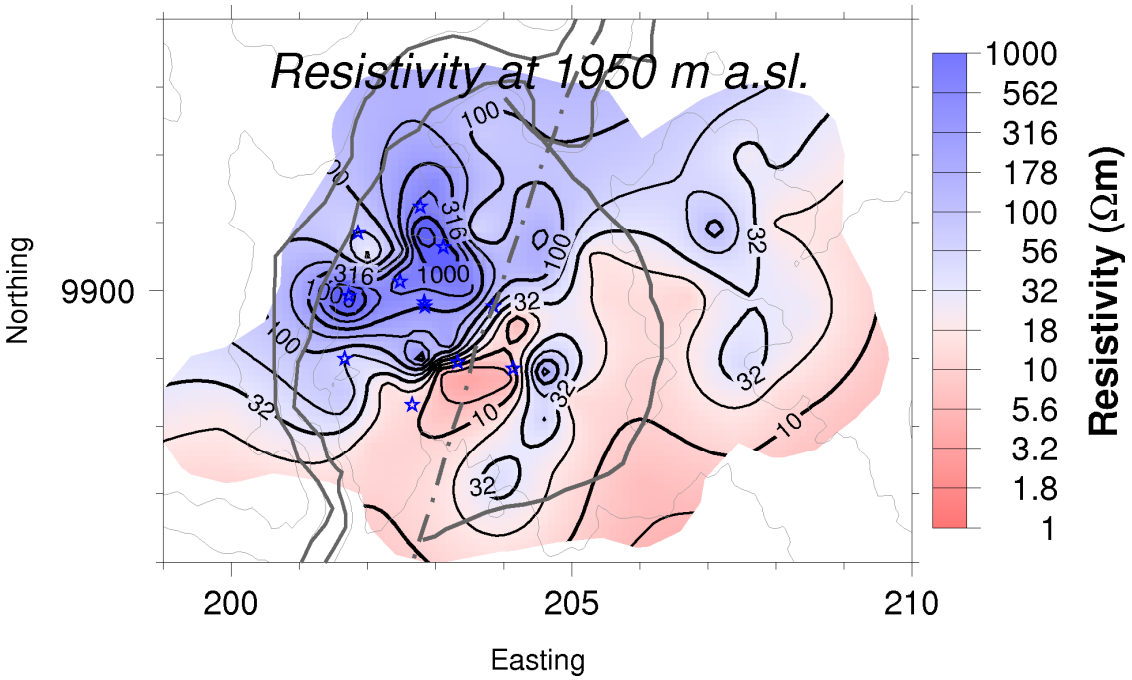

FIGURE 24: Resistivity in the Domes area at 1950 m a.s.l. according to joint 1-D inversion of TEM and MT data; the blue (gray) stars show the drilled wells in Domes while elevation contours and fault lines (see Figure 14) are seen in the background

A resistivity map at 1500 m a.s.l. is shown in Figure 26. The low resistivity has been smeared all over the study area at this depth. This low resistivity is associated with the alteration cap immediately on top of the high-resistivity core which probably reflects a zone where hydrothermal alteration products such as smectite and zeolites are abundant. High-resistivity anomalies are now appearing, one from the southwest and another furthest in the lower eastern sector of the field. These high-resistivity anomalies could probably be associated with the high-temperature alteration zone.

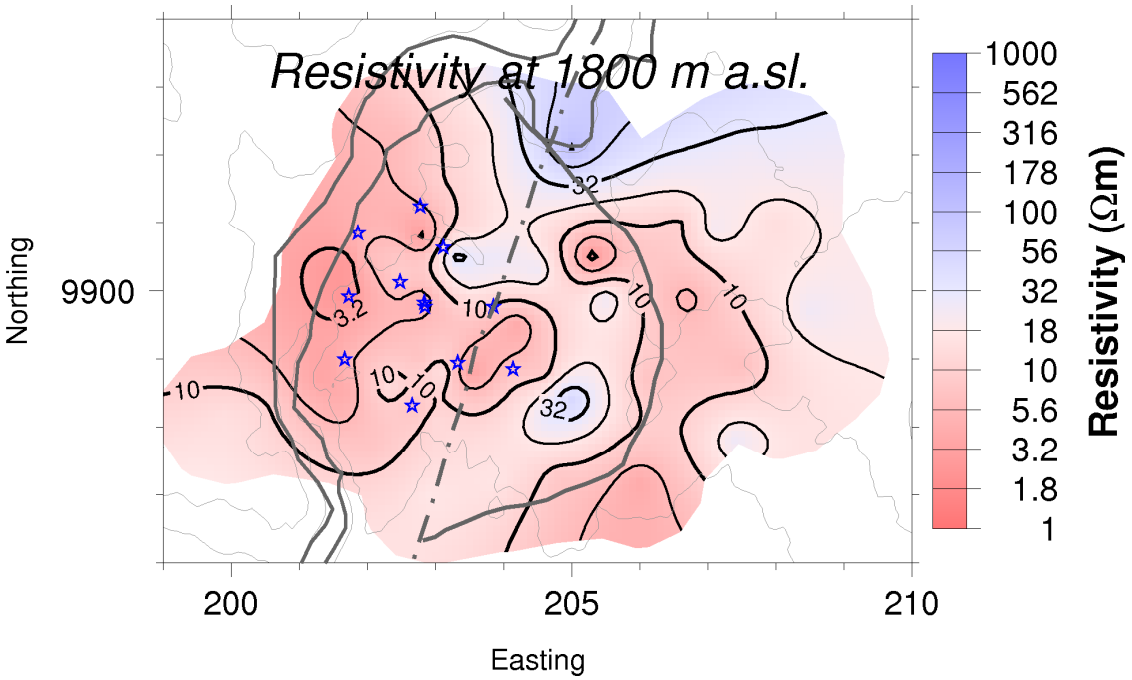

FIGURE 25: Resistivity in the Domes area at 1800 m a.s.l.

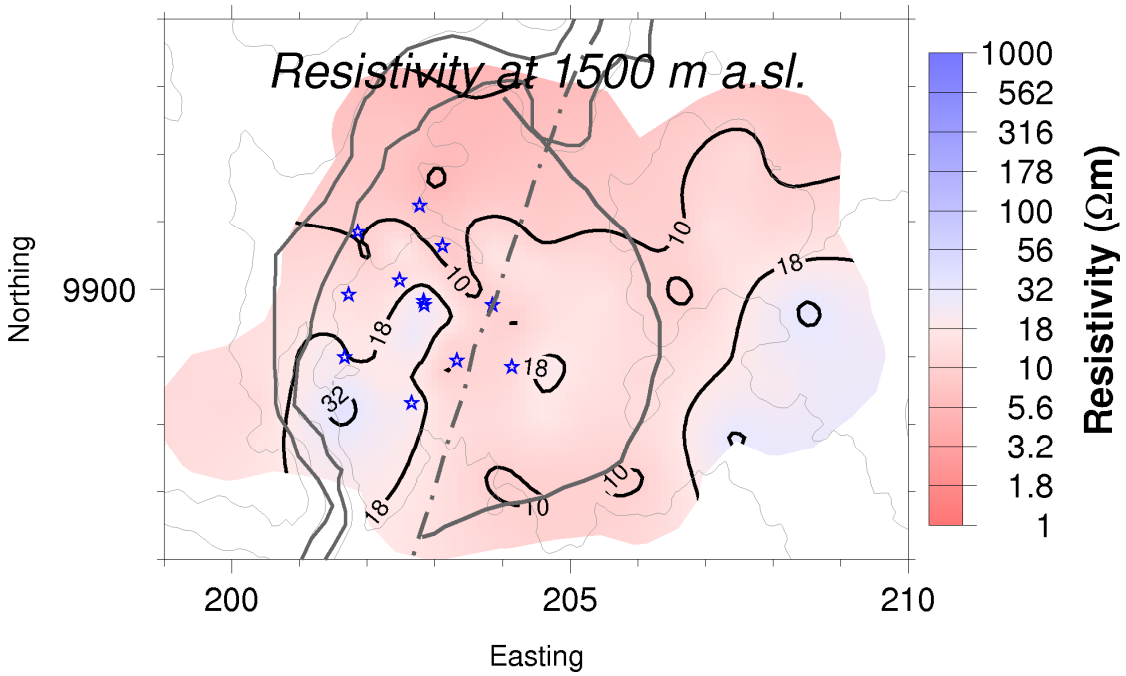

FIGURE 26: Resistivity in the Domes area at 1500 m a.s.l.

A resistivity map at 1000 m a.s.l. is shown in Figure 27. At this elevation high-temperature alteration (resistive core) is appearing from the west, central and eastern parts of the survey area. This high-resistivity core is probably the result of high-temperature minerals like epidote and chlorite. Low resistivities can still be seen in the north and northeast. A localised low-resistivity region is seen in the central part of the study area superimposed in between the high-resistivity structures. This could well reflect a fault-like structure.

A resistivity map at sea level is shown in Figure 28. At this depth the high-temperature alteration (resistive zone) has fully set in with more dominance in the central Domes area where wells have been drilled, and to the eastern sector of the survey area. This high resistivity perhaps reflects a relatively high-temperature zone where geothermal fluids may be prevalent. Superimposed on the high-resistivity core is a lower resistivity aligned in a NE-SW direction, which could probably be a zone of

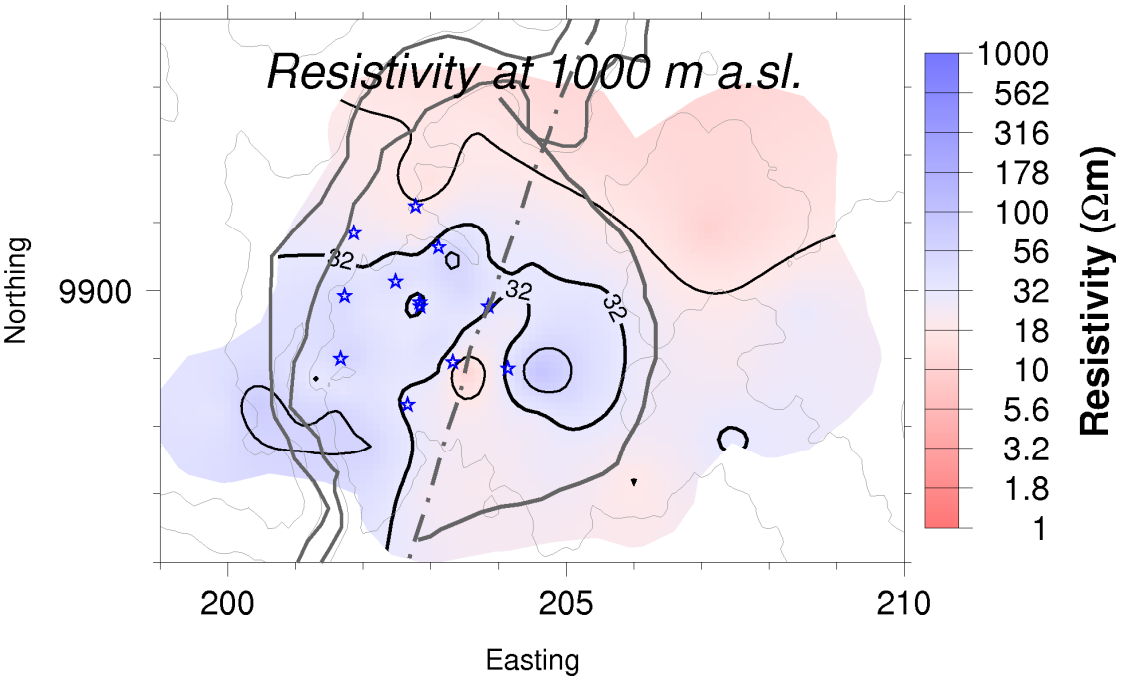

FIGURE 27: Resistivity in the Domes area at 1000 m a.s.l.

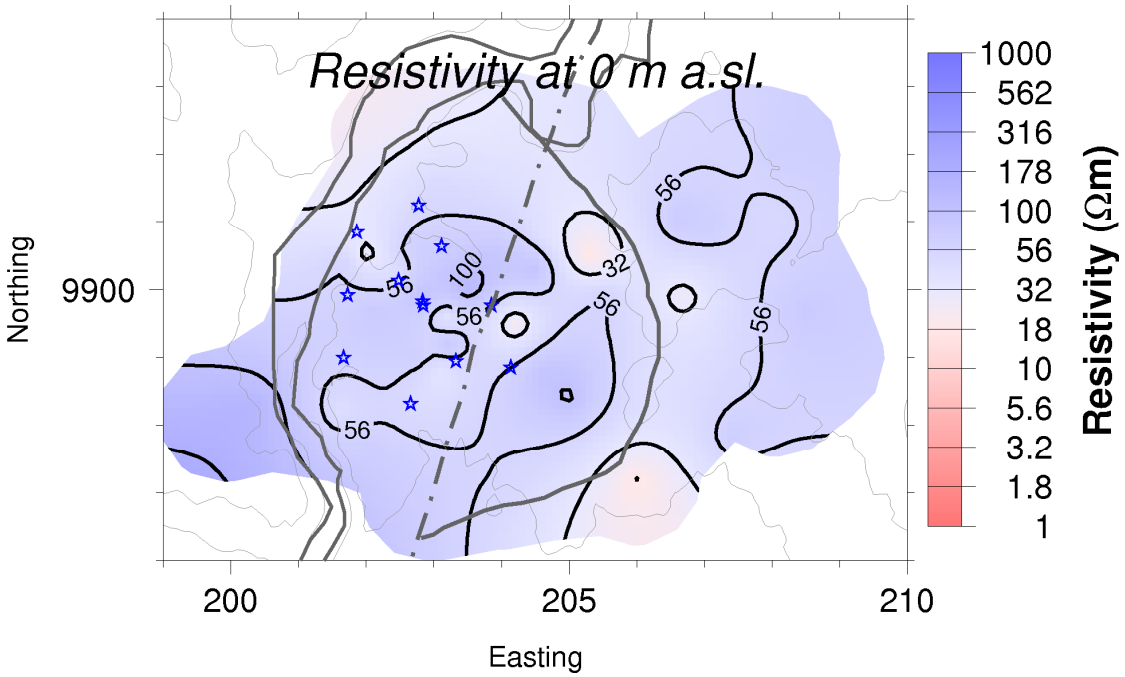

FIGURE 28: Resistivity in the Domes area at sea level

high permeability where hydrothermal alteration is not advanced, suggesting a possible up-flow zone beneath. An anomaly of medium to low resistivity is starting to show up between Easting 205 and 207, aligned in a North-South direction along the Domes ring structure.

A resistivity map at 1000 m b.s.l. is shown in Figure 29. The resistivity is still high in most of the survey area. The low-resistivity anomaly seen in the previous elevation is still present along the geological ring structure. A relatively low resistivity is also seen in the northwest sector of the study area, along the northern part of the Ol'Njorowa gorge.

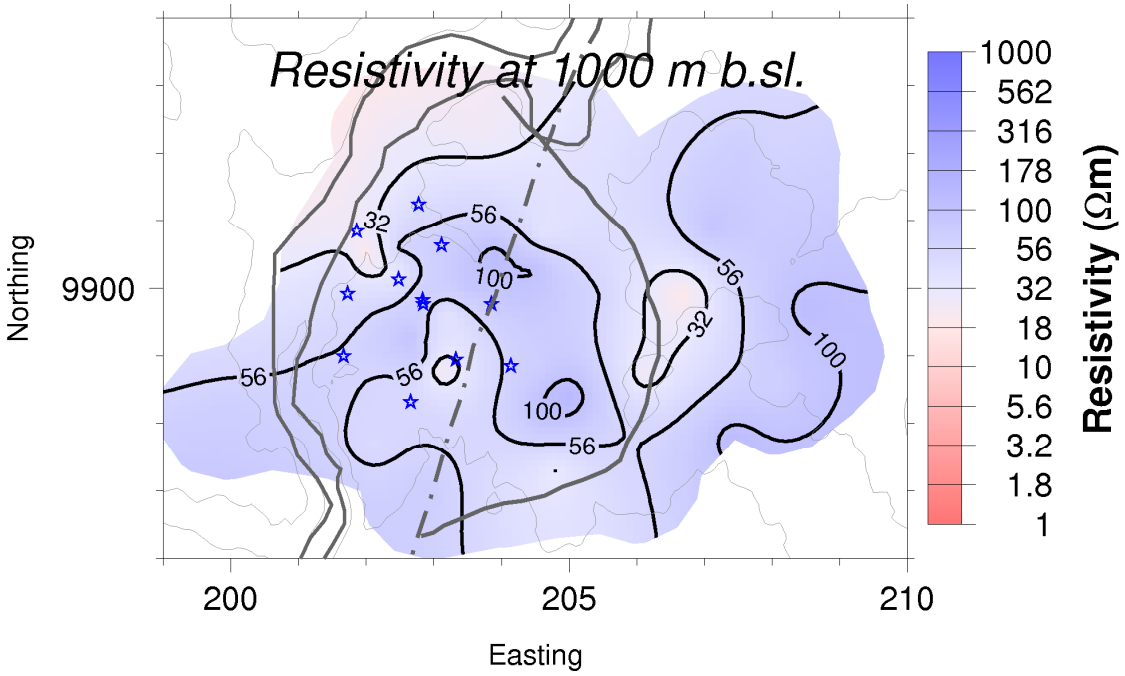

FIGURE 29: Resistivity in the Domes area at 1000 m b.s.l.

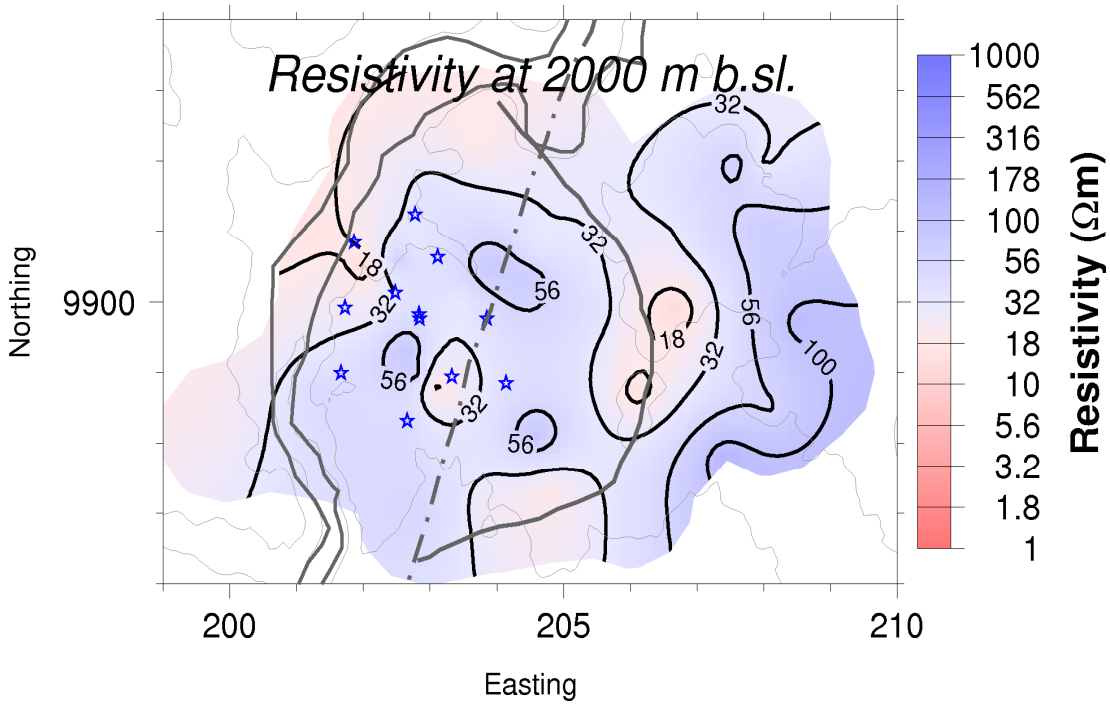

FIGURE 30: Resistivity in the Domes area at 2000 m b.s.l.

A resistivity map at 2000 m b.s.l. is shown in Figure 30. The high resistivity is still dominant in the central sector of Domes field and to the east. The low-resistivity anomalies seen at 1000 m b.s.l. are more expressed here, one to the west of the field running in a NNE-SSW direction along the Ol'Njorowa gorge and the other aligning in a N-S direction along the Domes ring structure.

A resistivity map at 5000 m b.s.l. is shown in Figure 31. At this depth the low resistivity is seen in almost the whole study area with the lowest resistivity (< 10 Ωm) aligning in a NNE-SSW direction. This low resistivity could be reflecting the heat source. However, it is not well observed in many MT sites due to the lack of long enough period data.

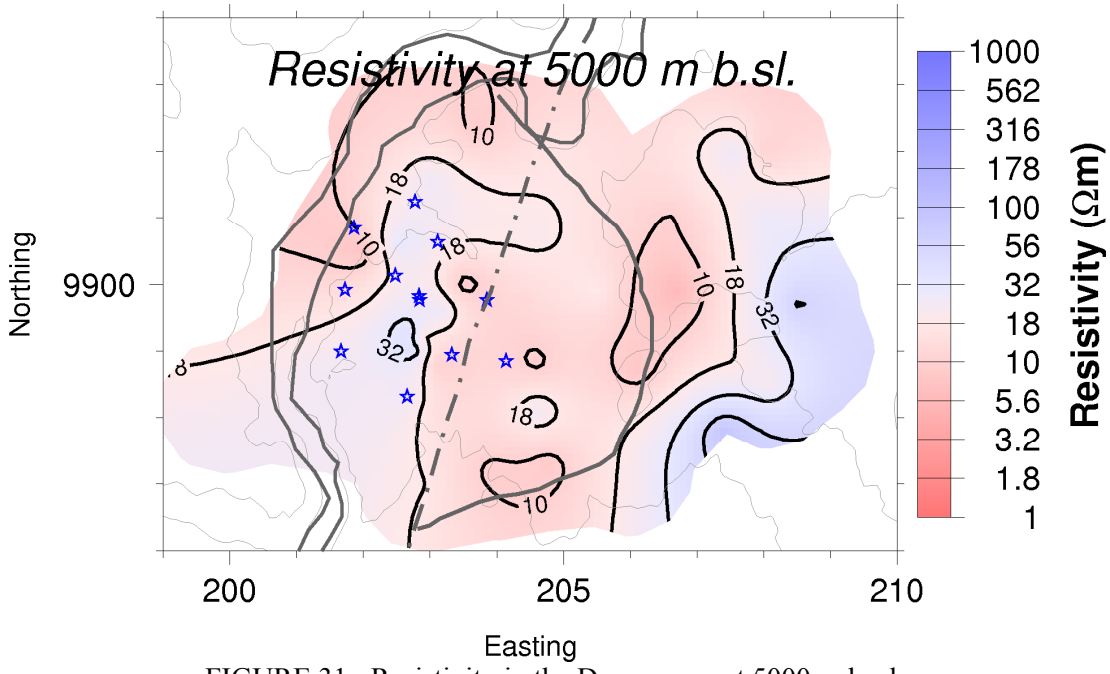

FIGURE 31: Resistivity in the Domes area at 5000 m b.s.l.

6.3 Correlation of the resistivity structure with well temperature data and alteration

This section describes the observed relationship between electrical resistivity, alteration mineralogy and reservoir temperatures. The data presented is temperature logs from wells 901-910 and lithology from wells 901, 902, 903, 904, 908A, 909 and 910.

Resistivity cross-section NWSE2 passing through wells 901, 904, 903, 908A and 909 is shown in Figure 32 with alteration mineralogy and temperature from those wells. Here, a low-resistivity zone of the order of 10 Ωm is observed between the surface high resistivity and the higher resistivity below at about 1-2 km depth. Five wells have been drilled along this profile showing the zones of dominant alteration minerals. Formation temperature isotherms, based on temperature logs from the wells are also projected into this profile. The figure shows very good correlation between the resistivity, temperature and alteration for wells 904, 903, 908A, and 909. The resistivity is high in the cold, unaltered rocks outside the reservoir and decreases considerably as geothermal alteration in the smectite-zeolite zone sets in. The bottom of this region correlates with temperature of about 100°C and resistivity of about 10 Ωm. At around the 200°C isotherm, the smectite-zeolite zone is slowly disappearing and is replaced by the mixed-layer clay zone, with resistivity in the range of 30 Ωm after which the resistivity increases considerably again and stays relatively high in the chlorite and chlorite-epidote zones at temperatures exceeding 250°C.

Well 901 also demonstrates a consistent correlation between the alteration mineral zones and resistivity. The low-resistivity cap (resistivity lower than 10 Ωm) coincides with the smectite-zeolite zone, which extends to about 800 m below the surface. In the chlorite-epidote zone there is also correlation between resistivity and alteration though the resistivity is not as high as in the high-resistivity core to the southeast. The correlation with temperature in the well (and partly also in well 904) is not as good, thus the alteration mineralogy is not in equilibrium with present temperature in the system which probably could be a result of heating having occurred in that zone.

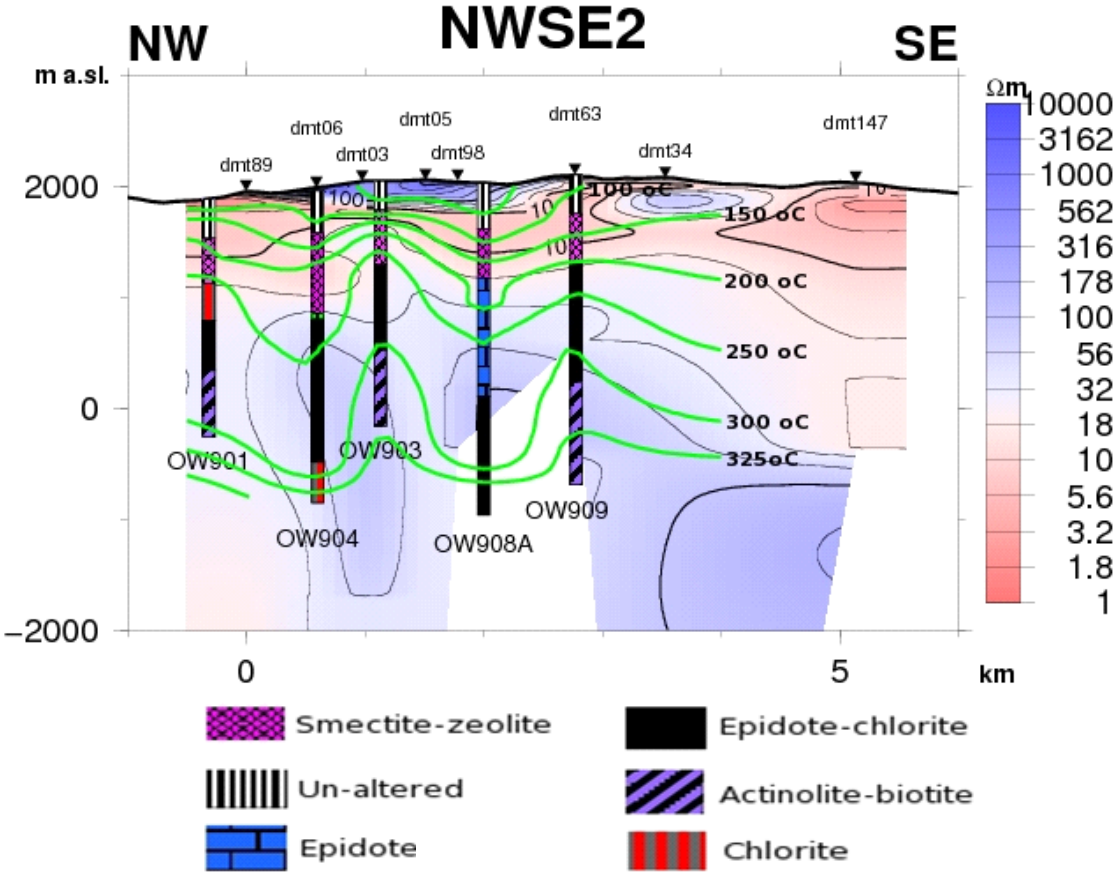

FIGURE 32: Resistivity cross-section NWSE2, alteration zoning in wells and well log temperature

Studies have shown that the appearance of hydrothermal minerals can be used as indicators of past or present temperature and at the same time becomes an indicator of the impermeable behaviour of geological units because of the sealing of open fractured spaces. Therefore, hydrothermal mineralogy can be used as a support in defining the extent of the reservoir.

7. DISCUSSION

In the Olkaria-Domes study area, 52 central-loop TEM soundings and 62 MT soundings were interpreted by 1-D joint inversion. The results were presented by iso-resistivity maps at different depths and resistivity cross-sections. The results showed fairly good correlation with the available geological information. The compiled resistivity model from the 1-D inversions reveals that the Domes geothermal area is generally characterized by a high-resistivity surface layer (> 100 Ωm), which is interpreted as fresh un-altered rocks possibly due to the thick pyroclastic cover from the adjacent Longonot volcano. Below that is a low-resistivity layer of about 10 Ωm which correlates very well with the mineral alteration of smectite-zeolite zone of the geothermal reservoir. This zone also correlates very well with temperatures in the range of 100-200°C.

Below the low-resistivity cap is a high-resistivity core which is evident in all the cross-sections within the study area. The existence of a high-resistivity core indicates reservoir temperatures exceeding 250°C, which has been confirmed by the drilled wells. Alteration mineralogy also is in agreement with a resistivity structure, confirmed by the presence of an epidote-chlorite zone. In the region around well OW901, the reservoir temperature is not in equilibrium with the alteration of the rocks.

The low resistivity seen at sea level in the middle zone of domes may be due to low-resistivity fluid in the pore spaces. Moreover, there is a consistency in the distribution of the zone of relatively low resistivity at depth (> 2 km b.s.l.) and the ring of domes' alignment in the Domes sector. Therefore, this zone of relatively low resistivity at depth possibly indicates a high-temperature zone representing a major source of crustal fluids.

Comparison of well data with the resistivity structure shows good correlation between the resistivity and alteration mineralogy. The low resistivity is dominated by conductive minerals in the smectite-zeolite zone at temperatures of 100-200°C. In the temperature range of 200-240°C, zeolites disappear and smectite is gradually replaced by resistive chlorite. At temperatures exceeding 250°C, chlorite and epidote are the dominant minerals and the resistivity is probably dominated by the pore fluid conduction in the high-resistivity core.

8. CONCLUSIONS AND RECOMMENDATION

Results from the resistivity cross-sections derived from the 1-D joint MT and TEM inversions in the Domes area reveal four main layers, namely: a very shallow high-resistivity layer of > 100 Ωm, an intermediate low-resistivity layer of < 10 Ωm underlying the upper high-resistivity layer, and a deep high-resistivity layer with values greater than 50 Ωm underlying the low-resistivity layer. Further down, at a few kilometres depth below sea level, there is a low-resistivity zone that could relate to the heat source for the geothermal system.

Based on these results it can be concluded that the Domes geothermal field hosts a much larger geothermal system than previously thought. The system appears to cover a much larger area than the coverage of the soundings. If there is equilibrium between the hydrothermal alteration of the rock and the present temperature in the reservoir, then the temperature in the high-resistivity core is expected to be more than 250°C, as evidenced from the well data.

It is recommended that more long period MT and TEM data at the same location be acquired in order to define the extent of the Domes field and 3-D interpretation be carried out to define three-dimensional features both laterally and at depth. It is also important to measure TEM data at those MT sites where no TEM data exist.

ACKNOWLEDGEMENTS

I would like to express my gratitude to the UNU-GTP and the Government of Iceland for awarding me this scholarship to participate in the six months training programme. Special thanks go to Dr. Ingvar Birgir Fridleifsson, the director, Mr. Lúdvík S. Georgsson, Ms. Dorthe H. Holm, Ms. Thórhildur Ísberg and Mr. Markús A.G. Wilde, and all of UNU staff for their superb coordination of the training activities and for being available to give guidance and help whenever I needed it. I am sincerely grateful to you all. I feel honoured to have been a student of my supervisor, Dr. Hjálmar Eysteinsson, who tirelessly guided me throughout this research work and shared with me lots of valuable knowledge. My sincere appreciation goes to the ISOR geophysics team for their tireless guidance throughout the specialised training and project work, Mr. Knútur Árnason was always there for me whenever I needed his advice.

I am grateful to my employer the Kenya Electricity Generating Company Ltd. – KenGen for providing data used in this study and granting me leave to undertake this course. Special thanks go to Cornel Ofwona for availing reservoir data and Peter Mbia for providing well lithological data for use in this project. To my colleagues at the geophysics office, I thank you so much for your support throughout this course. To the 2009 UNU fellows I say, thank you very much for the wonderful time and discussions that we shared together. To my beloved wife Joyce and sons Arnold, Emmanuel and Trevis, words are not enough to express my sincere thanks to you for enduring my absence, for your love and prayers throughout my entire stay in Iceland. May God bless you.

REFERENCES

Árnason, K., 1989: *Central-loop transient electromagnetic sounding over a horizontally layered earth*. Orkustofnun, Reykjavík, report OS-89032/JHD-06, 129 pp.

Árnason, K., 2006: *TEMTD, a programme for 1-D inversion of central-loop TEM and MT data. Short manual*. ÍSOR – Iceland GeoSurvey, Reykjavík, internal report, 17 pp.

Árnason, K., 2008: *The magneto-telluric static shift problem*. ÍSOR – Iceland GeoSurvey, Reykjavík, report, ISOR-08088, 17 pp.

Árnason, K., Karlsdóttir, R., Eysteinsson, H., Flóvenz, Ó.G., and Gudlaugsson, S.Th., 2000: The resistivity structure of high-temperature geothermal systems in Iceland. *Proceedings of the World Geothermal Congress 2000*, *Kyushu-Tohoku, Japan,* 923-928.

Brace, W.F., and Orange A.S. 1968: Further studies of the effects of pressure on electrical resistivity of rocks. *J. Geophys. Res., 73-16,* 5407–5420.

Christensen, A., Auken, E., and Sørensen, K., 2006. The transient electromagnetic method. *Groundwater Geophysics, 71*, 179-225.

Clarke, M.C.G., Woodhall, D.G., Allen, D., and Darling, G., 1990: *Geological, volcanological and hydrogeological controls of the occurrence of geothermal activity in the area surrounding Lake Naivasha, Kenya*. Ministry of Energy, Nairobi, report 150, 138 pp.

Dakhnov, V.N., 1962: Geophysical well logging. *Q. Colorado Sch. Mines, 57-2*, 445 pp.

DeGroot-Hedlin, G., 1991. Removal of static shift in 2 dimensions by regularized inversion. *Geophysics, 56,* 2102-2106.

Eysteinsson, H., 1998: *TEMMAP and TEMCROSS plotting programs*. ÍSOR – Iceland GeoSurvey, Unpublished programs and manuals.

Hermance, J.F., 1973: Processing of magnetotelluric data. *Physics of the Earth and Planetary Interiors, 7,* 349-364.

Jones, A.G., 1988: Static shift of magnetotelluric data and its removal in a sedimentary basin environment. *Geophysics, 53-7*, 967-978.

Hersir, G.P., and Björnsson, A., 1991: *Geophysical exploration for geothermal resources. Principles and applications*. UNU-GTP, Iceland, report 15, 94 pp.

Kearey, P., and Brooks, M., 1994: *An introduction to geophysical exploration* (2nd edition). Blackwell Scientific Publ., London, 236 pp.

Keller, G.V., and Frischknecht, F.C., 1966: *Electrical methods in geophysical prospecting.* Pergamon Press Ltd., Oxford, 527 pp.

Lagat, J.K., 2004: *Geology, hydrothermal alteration and fluid inclusion studies of the Olkaria Domes geothermal field, Kenya.* University of Iceland, MSc thesis, UNU-GTP, Iceland, report 2, 71 pp.

Lee Lerner, K., Lerner, B.W., and Cengage, G., 2003: *Porosity and permeability.* World of Earth Science, webpage: http://www.enotes.com/earth-science/

Lichoro, C.M., 2009: *Appendices to the report "Joint 1-D inversion of TEM and MT data from Olkaria Domes geothermal area, Kenya."* UTP-GTP, Iceland, report 16, appendices, 45 pp.

Muchemi, G.G., 1992: *Structural map of Olkaria geothermal field showing inferred ring structures.* Kenya Power Company, internal report, 27 pp.

Mungania, J., 1992: *Geology of the Olkaria geothermal complex.* Kenya Power Company Ltd., internal report, 38 pp.

Mungania J., 1999: *Summary of the updates of the geology of Olkaria Domes geothermal field.* KenGen, internal report.

Naylor, W.I., 1972: *Geology of the Eburru and Olkaria prospects.* U.N. Geothermal Exploration Project, report.

Ogawa, Y and Ushida, T., 1996: A two-dimensional magnetotelluric inversion assuming Gaussian static shift. *Geopys. J. Int., 126*, 69-76.

Omenda, P.A., 2000: Anatectic origin for comendite in Olkaria geothermal field, Kenya Rift; Geochemical evidence for syenitic protholith. *African J. Sci. & Technol., Science & Engineering Series, 1,* 39-47.

Quist, A.S., and Marshall, W.L., 1968: Electrical conductances of aqueous sodium chloride solutions from 0 to 800°C and at pressures to 4000 bars. *J. Phys. Chem., 72,* 684-703.

Simiyu, S.M., Oduong, E.O., and Mboya, T.K., 1998: *Shear wave attenuation beneath the Olkaria volcanic field*. KenGen, internal report.

Sternberg, B.K., Washburne, J.C., and Pellerin, L., 1988: Correction for the static shift in magnetotellurics using transient electromagnetic soundings. *Geophysics, 53,* 1459-1468.

Virkir, 1980: *Geothermal development at Olkaria*. Virkir Consulting Engineers, report prepared for Kenya Power Company.